Tripodal halogen bonding iodo-azolium receptors for anion recognition

Sheila Ruiz-Botella,[a] Pietro Vidossich,[b] Gregori Ujaque[b]*, Eduardo Peris[a]* and Paul. D. Beer[c*]

[a] Institute of Advanced Materials (INAM). Universitat Jaume I

Avda. Sos Baynat. 12071-Castellón. Spain.

E-mail: eperis@uji.es

[b]Departament de Química. Universitat Autónoma de Barcelona

08193-Cerdanyola del Vallès, Catalonia, Spain. E-mail: gregori.ujaque@uab.cat

[c] Department of Chemistry, Inorganic Chemistry Laboratory, University of Oxford, South Parks Road,

Oxford OX1 3QR, UK. E-mail: paul.beer@chem.ox.ac.uk.

S1. Nuclear Magnetic Resonance (NMR)

^{1}H Compound A

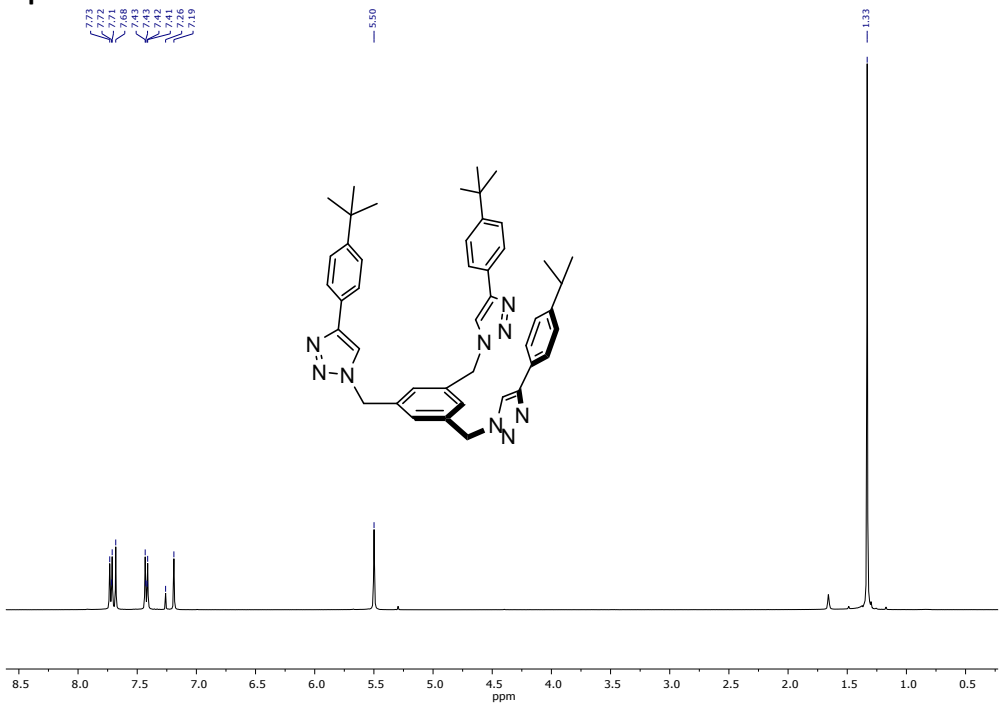

Figure S1. ^{1}H NMR (400 MHz, $CDCl_3$) δ 7.72 (d, *J* = 8.3 Hz, 8H, C*H*$_{benz}$), 7.68 (s, 3H, C*H*$_{benz}$), 7.42 (d, *J* = 8.4 Hz, 8H, C*H*$_{benz}$), 7.19 (s, 3H, C*H*$_{triaz}$), 5.50 (s, 6H, C*H*$_2$), 1.33 (s, 81H, C*H*$_3$).

^{13}C{1H}Compound A

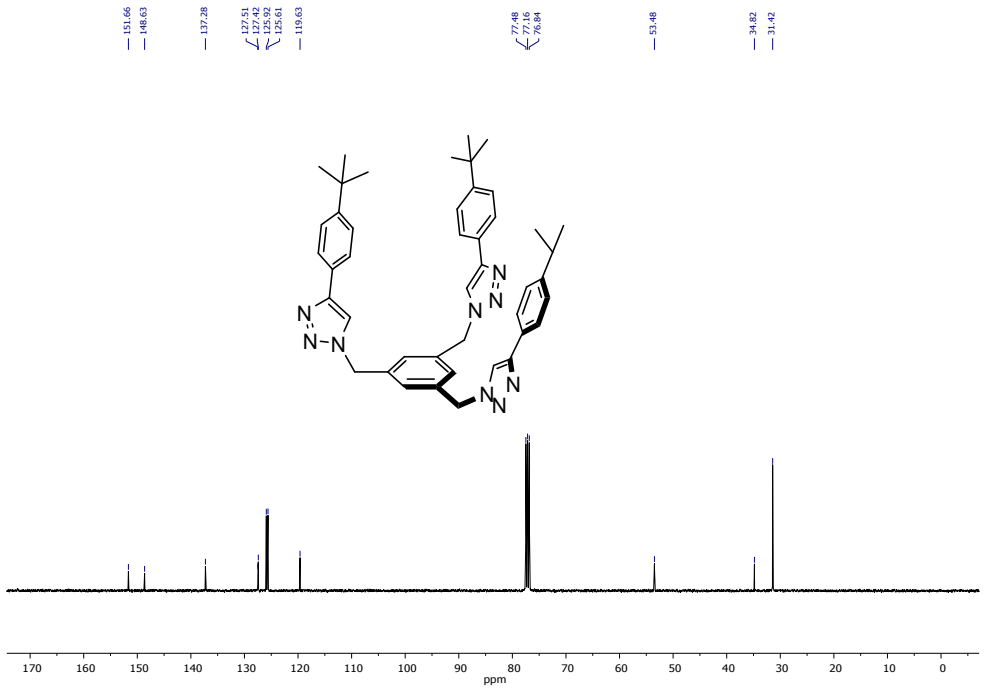

Figure S2. ^{13}C NMR (101 MHz, $CDCl_3$) δ 151.66, 148.63, 137.28, 127.51, 127.42, 125.92, 125.61, 119.63, 53.48, 34.82, 31.42.

^{1}H Compound B

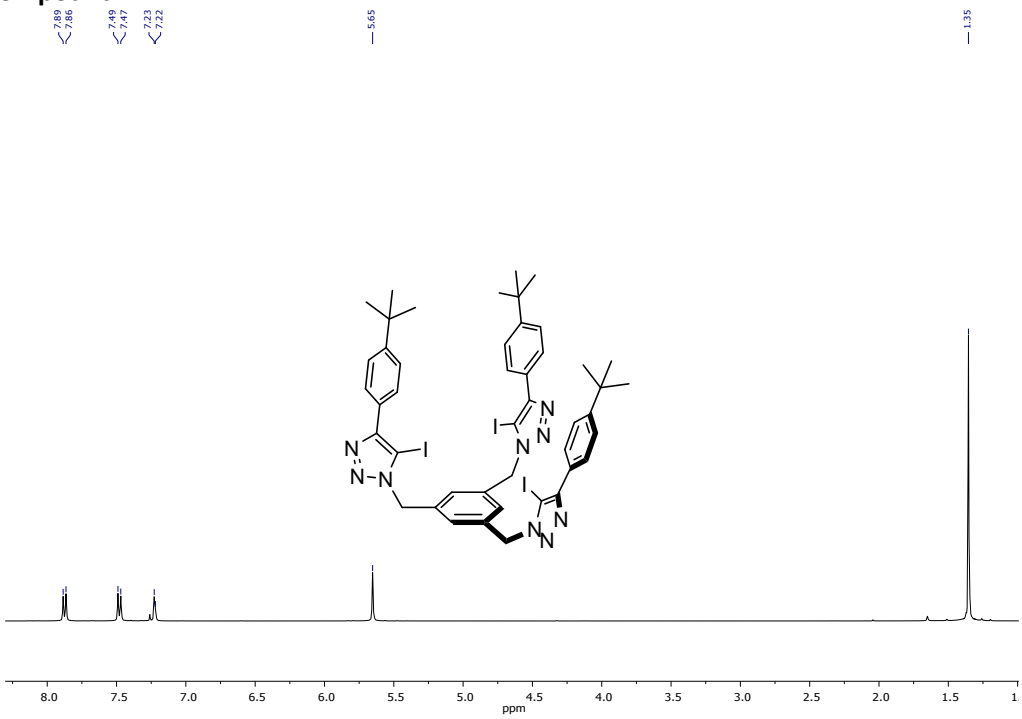

Figure S3. ^{1}H NMR (400 MHz, $CDCl_3$) δ 7.87 (d, *J* = 8.2 Hz, 6H, C*H*$_{benz}$), 7.48 (d, *J* = 8.2 Hz,6H, C*H*$_{benz}$), 7.23 (s, 3H, C*H*$_{benz}$), 5.65 (s, 6H, C*H*$_2$), 1.35 (s, 27H, C*H*$_3$).

^{13}C{1H}Compound B

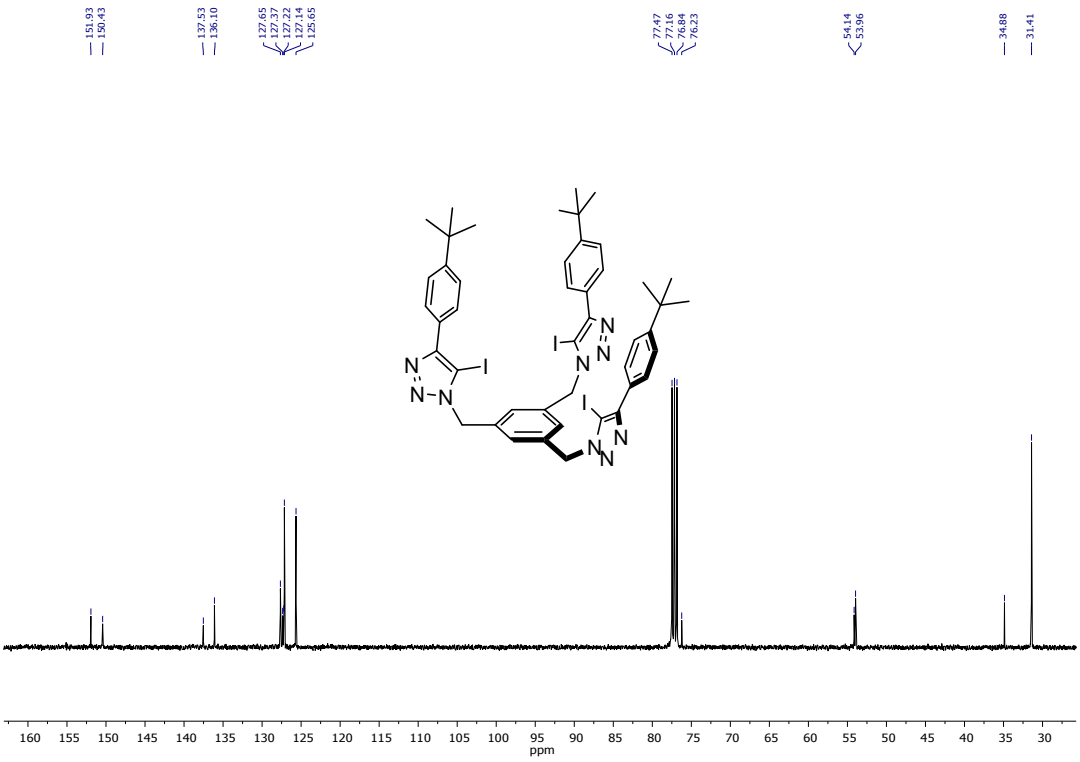

Figure S4. ^{13}C NMR (101 MHz, $CDCl_3$) δ 151.93, 150.43, 137.53, 136.10, 127.65, 127.37, 127.22, 127.14, 125.65, 76.23, 54.14, 53.96, 34.88.

^{1}H Compound C

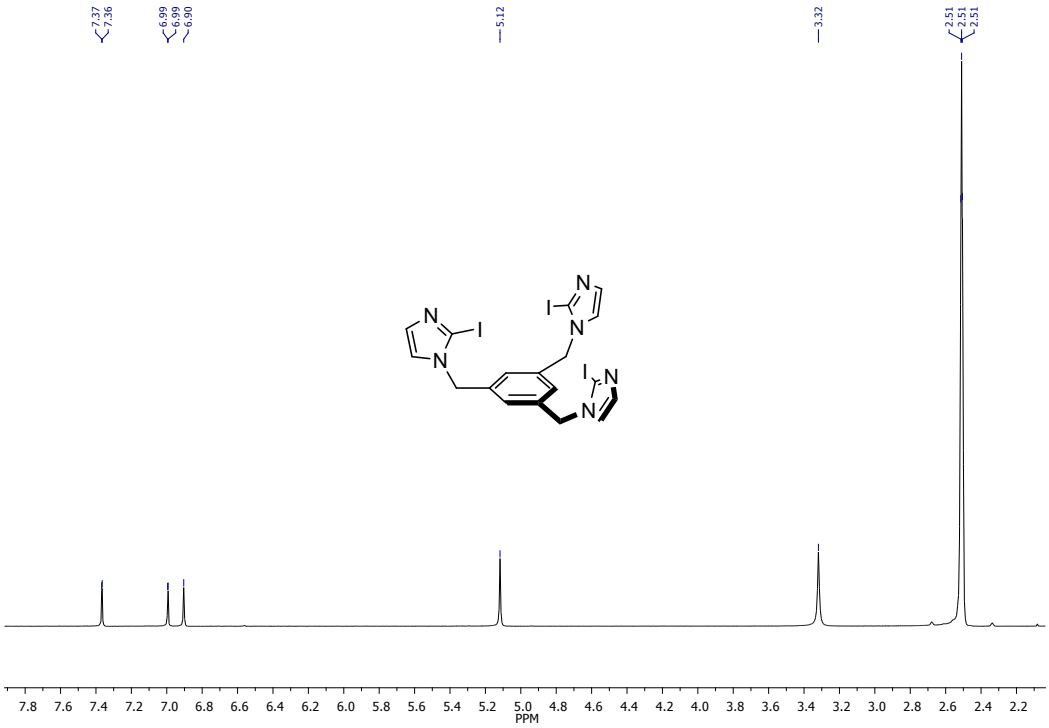

Figure S5.^{1}H NMR (400 MHz, DMSO-d^6) δ 7.37 (s, 3H, CH_{benz}), 6.99 (d, 3H, C*H*), 6.90 (d, 3H, C*H*), 5.12 (s, 6H, CH_2).

^{13}C{1H}Compound C

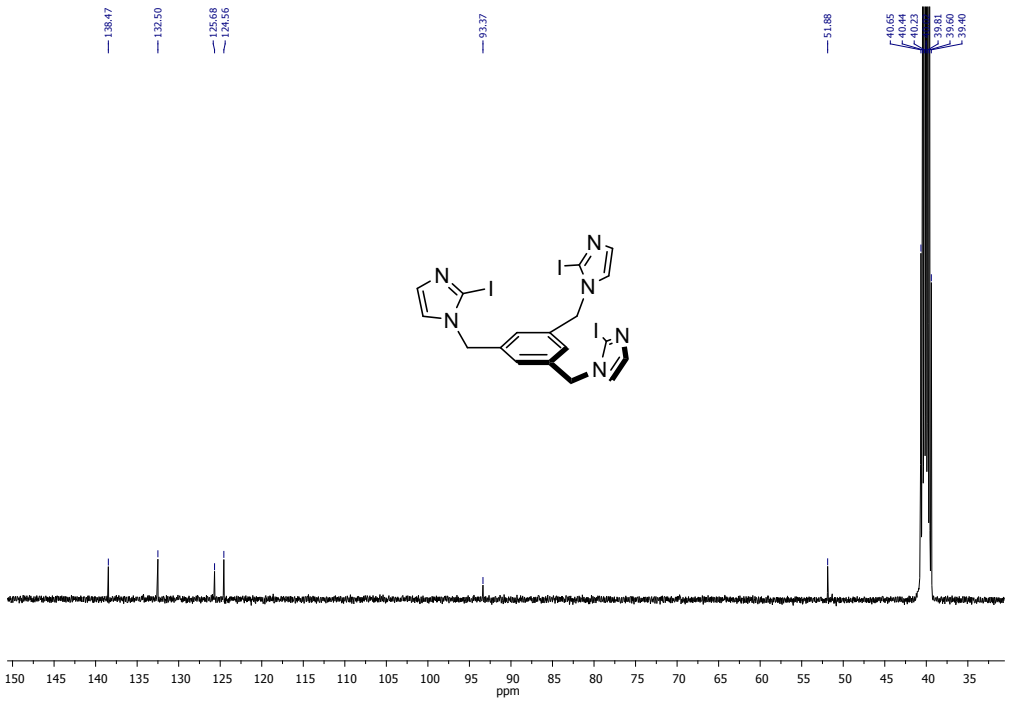

Figure S6.^{13}C NMR (101 MHz, DMSO-d^6) δ 138.47, 132.50, 125.68, 124.56, 93.37, 51.88, 40.65, 40.44, 40.23, 40.02, 39.81, 39.60, 39.40.

^{1}H Compound [2-H](PF$_6$)

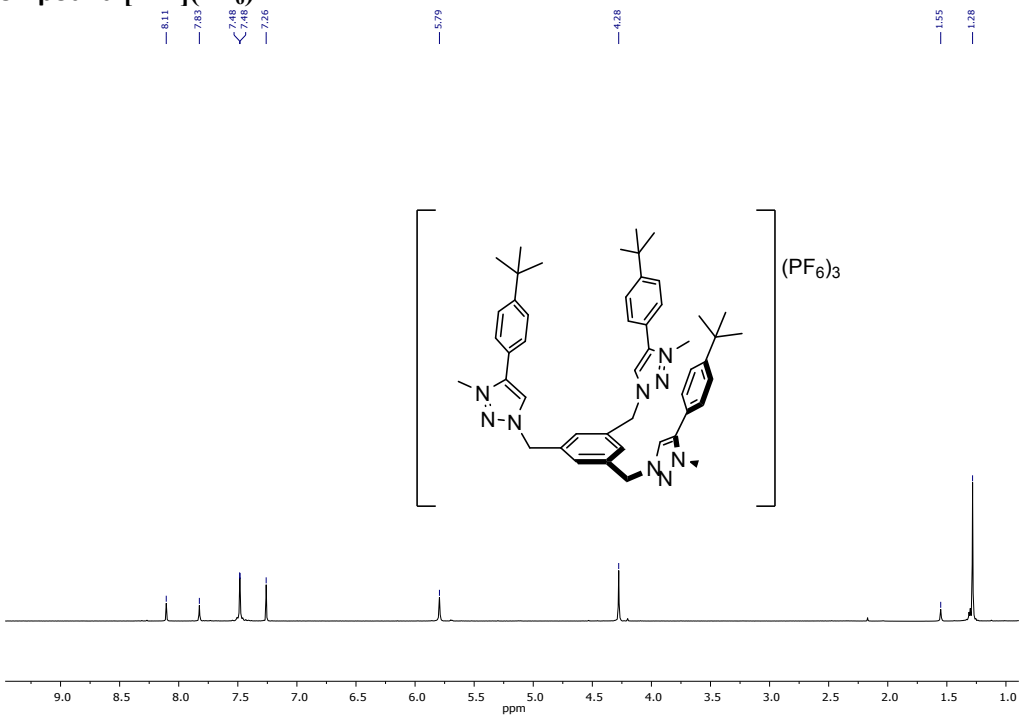

Figure S7. ^{1}H NMR (400 MHz, $CDCl_3$): δ 8.11(s, 3H, C*H*$_{triz}$), 7.83(s, 3H, C*H*$_{benz}$), 7.48 (broad signal, 12H, C*H*$_{benz,}$), 5.79(s, 6H, C*H*$_2$), 4.28 (s, 9H, C*H*$_3$), 1.28(s, 27H, C*H*$_3$).

^{13}C{1H}Compound [2-H](PF$_6$)

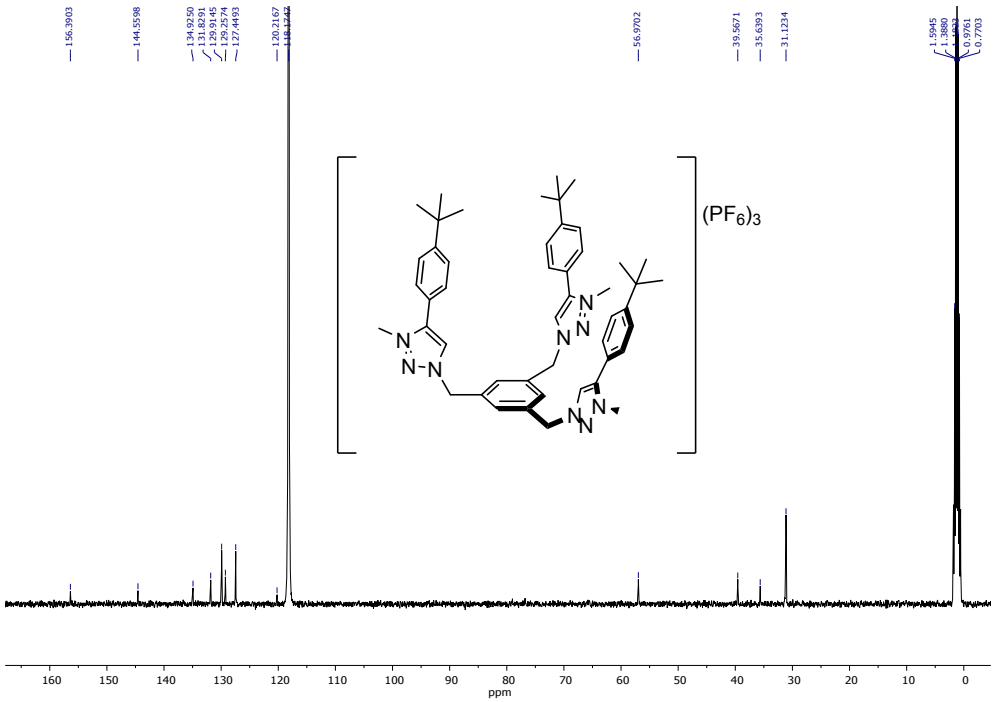

Figure S8. ^{13}C NMR (101 MHz, CD_3CN) δ 156.39, 144.56, 134.93, 131.83, 129.91, 129.26, 127.45, 120.22, 56.97, 39.57, 35.64, 31.12.

^{1}H Compound [2-I](PF$_6$)

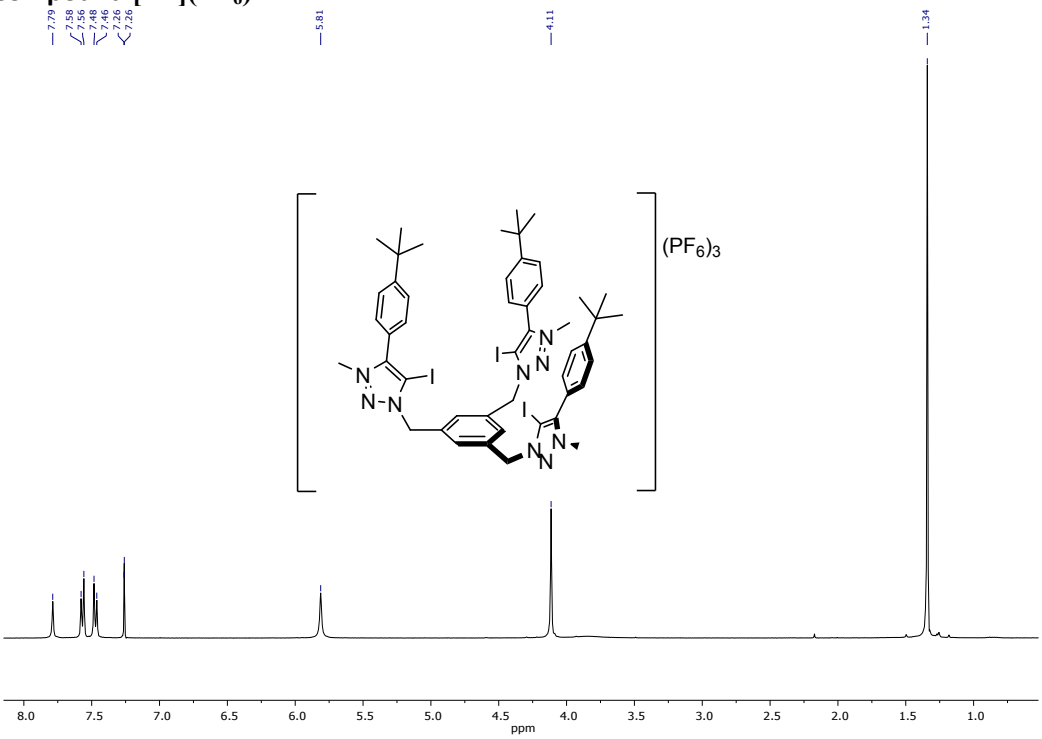

Figure S9. ^{1}H NMR (400 MHz, $CDCl_3$) δ 7.79 (s, 3H, C*H*$_{triaz}$), 7.57 (d, *J* = 8.2 Hz, 6H, C*H*$_{benz}$), 7.47 (d, *J* = 8.1 Hz, 6H, C*H*$_{benz}$), 5.81 (s, 6H, C*H*$_2$), 4.11 (s, 9H, C*H*$_3$), 1.34 (s, 27H, C*H*$_3$).

^{13}C{1H}Compound [2-I](PF$_6$)

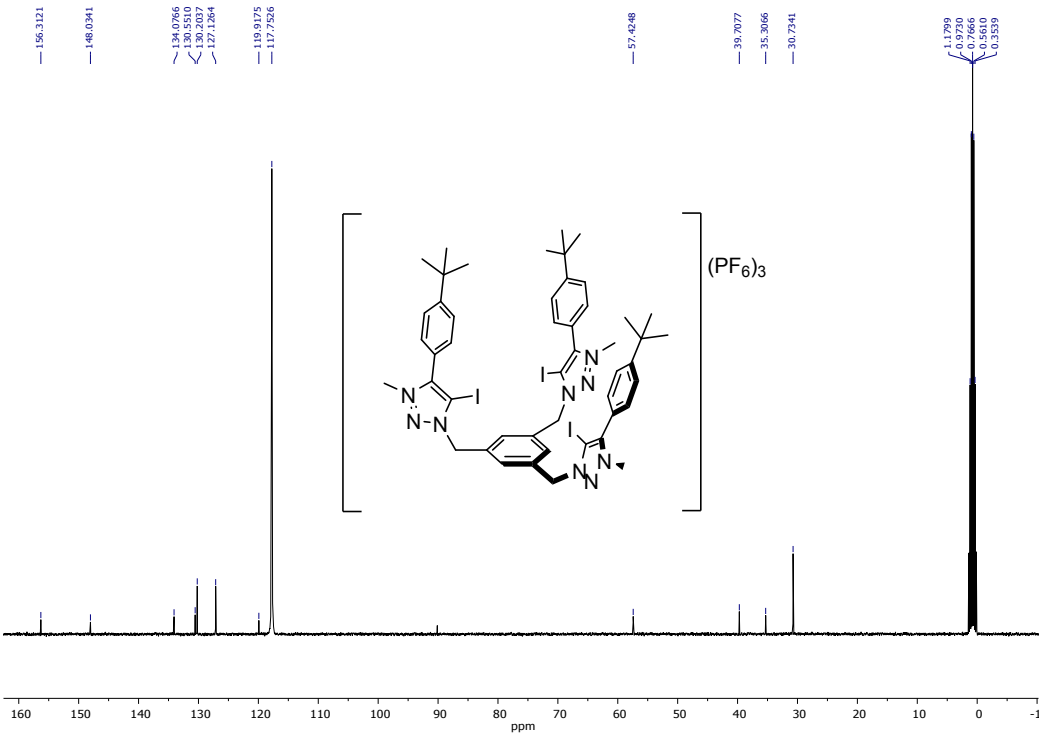

Figure S10. ^{13}C NMR (101 MHz, CD_3CN) δ 156.31, 148.03, 134.08, 130.55, 130.20, 127.13, 119.92, 57.42, 39.71, 35.31, 30.73.

^{1}H Compound [1-I](PF$_6$)

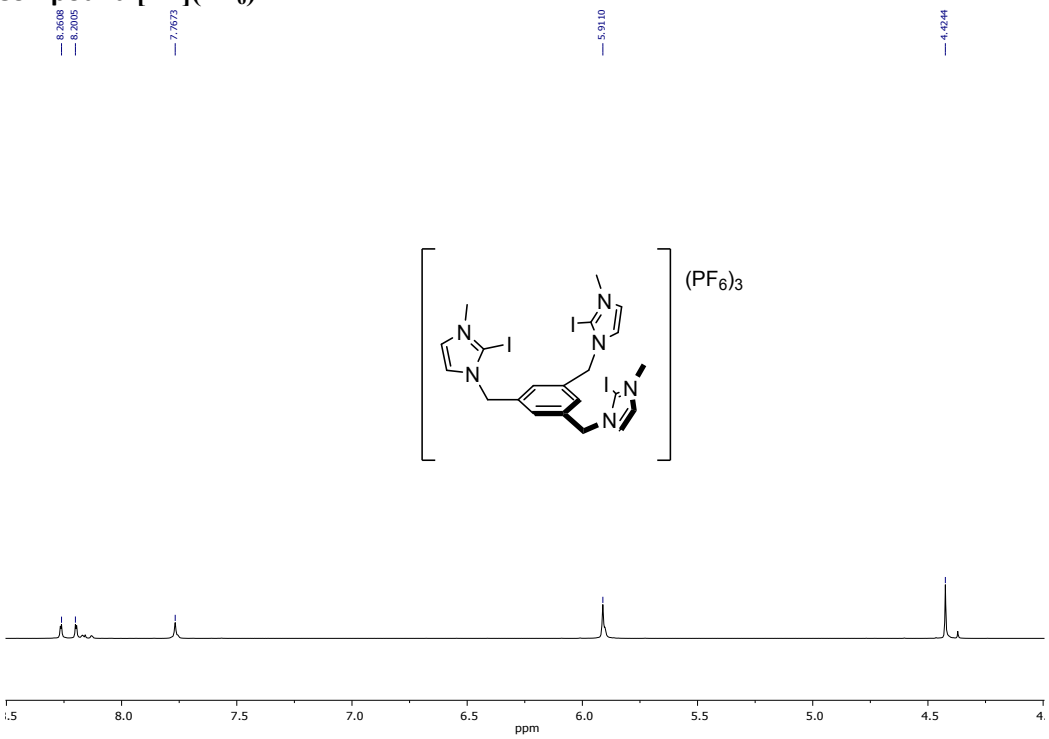

Figure S11. ^{1}H NMR (400 MHz, DMSO-d^6) δ 8.26 (d, 3H, C*H*), 8.20 (d, 3H, C*H*), 7.77 (s, 3H, C$H_{aromatic}$), 5.91 (s, 6H, CH_2), 4.42 (s, 9H, CH_3).

^{13}C{1H}Compound [1-I](PF$_6$)

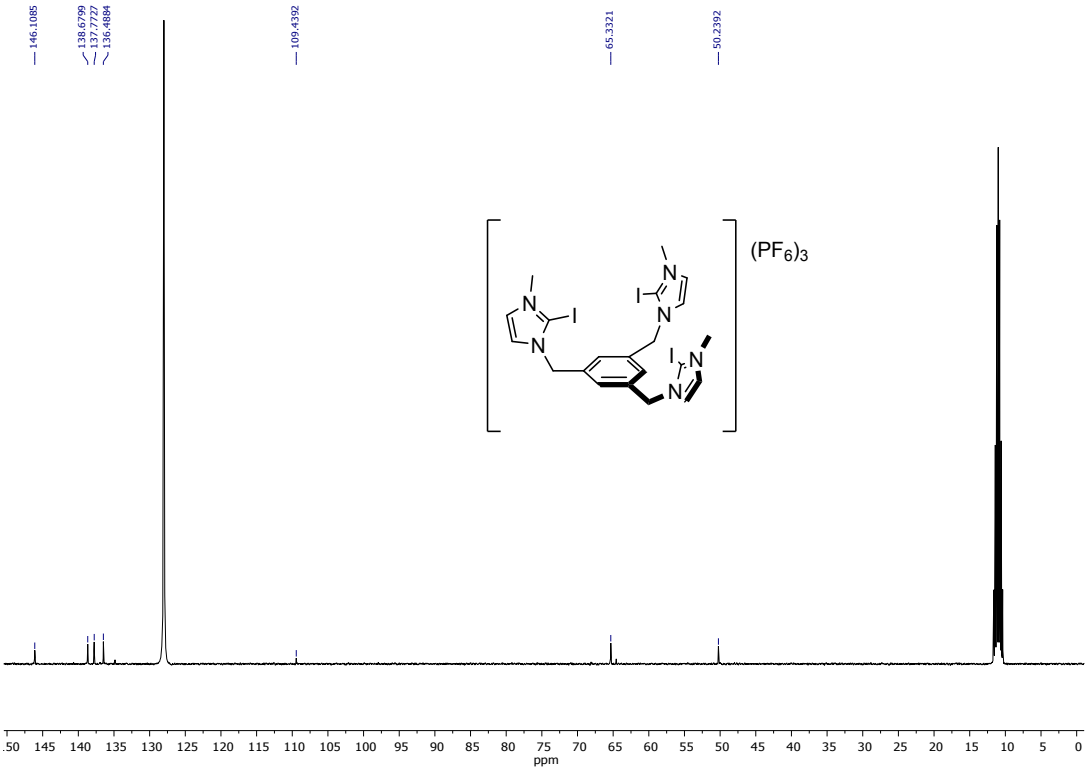

Figure S12. ^{13}C NMR (101 MHz, CD_3CN) δ 146.11, 138.68, 137.77, 136.49, 109.44, 65.33, 50.24.

S2. HIGH RESOLUTION MASS SPECTROMETRY

Compound A

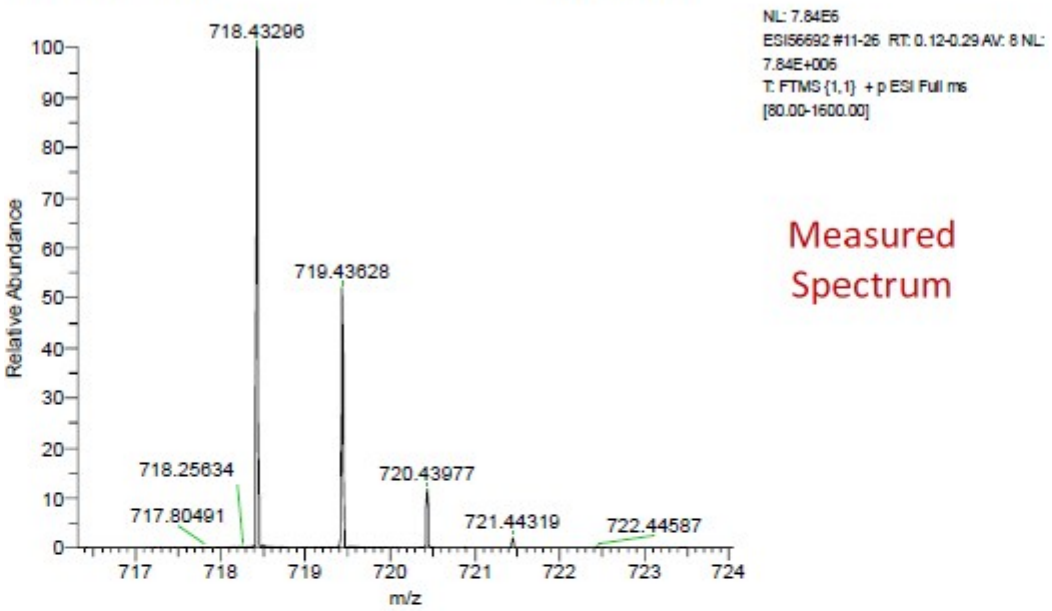

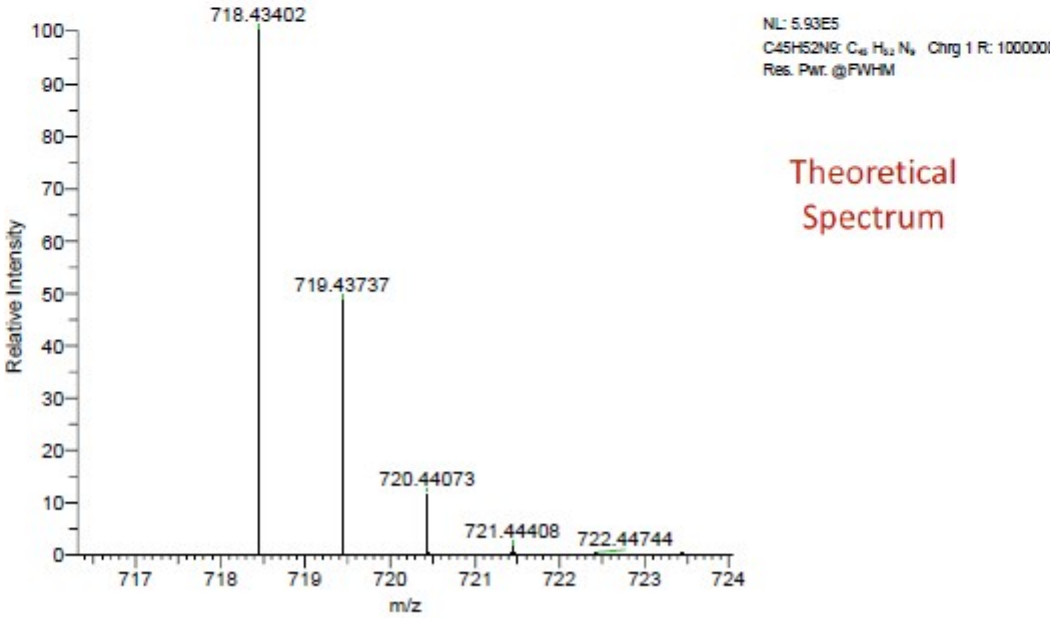

m/z	Formula	RDB	Delta ppm	Theo. Mass
718.43298	$C_{45}H_{52}N_9$	24.5	-1.44	718.43402

Figure S13

Compound B

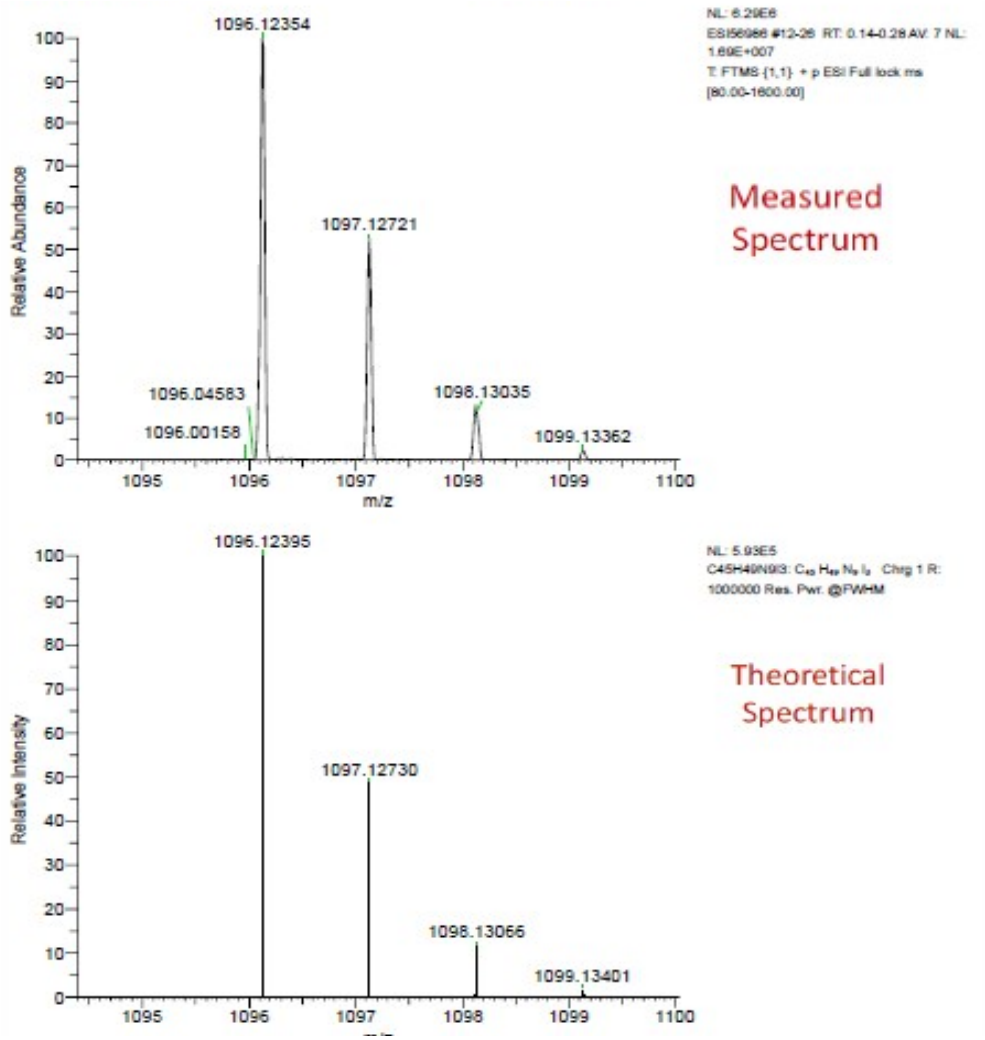

m/z	Formula	RDB	Delta ppm	Theo. Mass
1096.12354	$C_{45}H_{49}N_9{}^{127}I_3$	24.5	-0.38	1096.12395

Figure S14

Compound [2-H](PF_6)

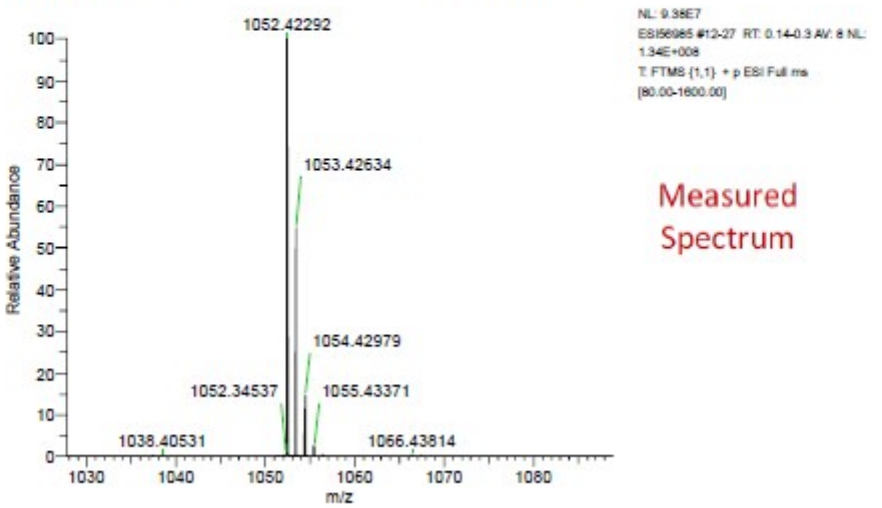

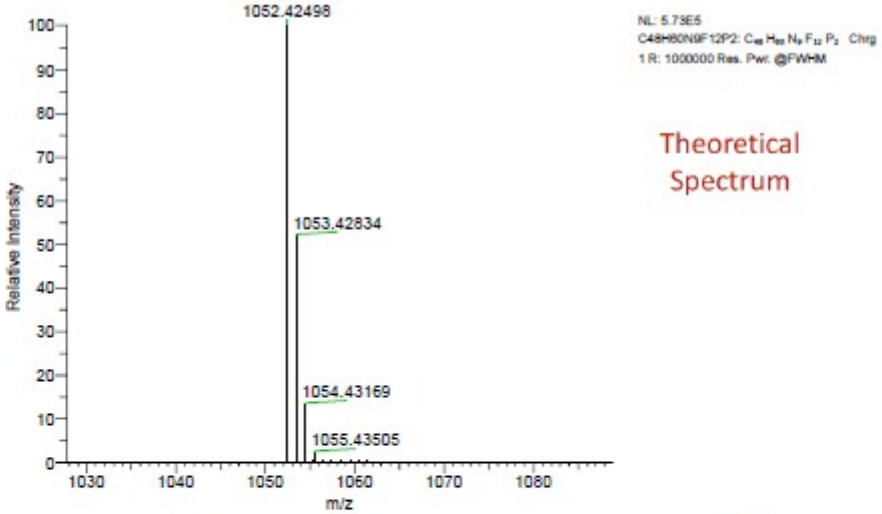

m/z	Formula	RDB	Delta ppm	Theo. Mass
1052.42297	$C_{48}H_{60}N_9F_{12}P_2$	18.5	-1.91	1052.42498

Figure S15

Compound [2-I](PF_6)

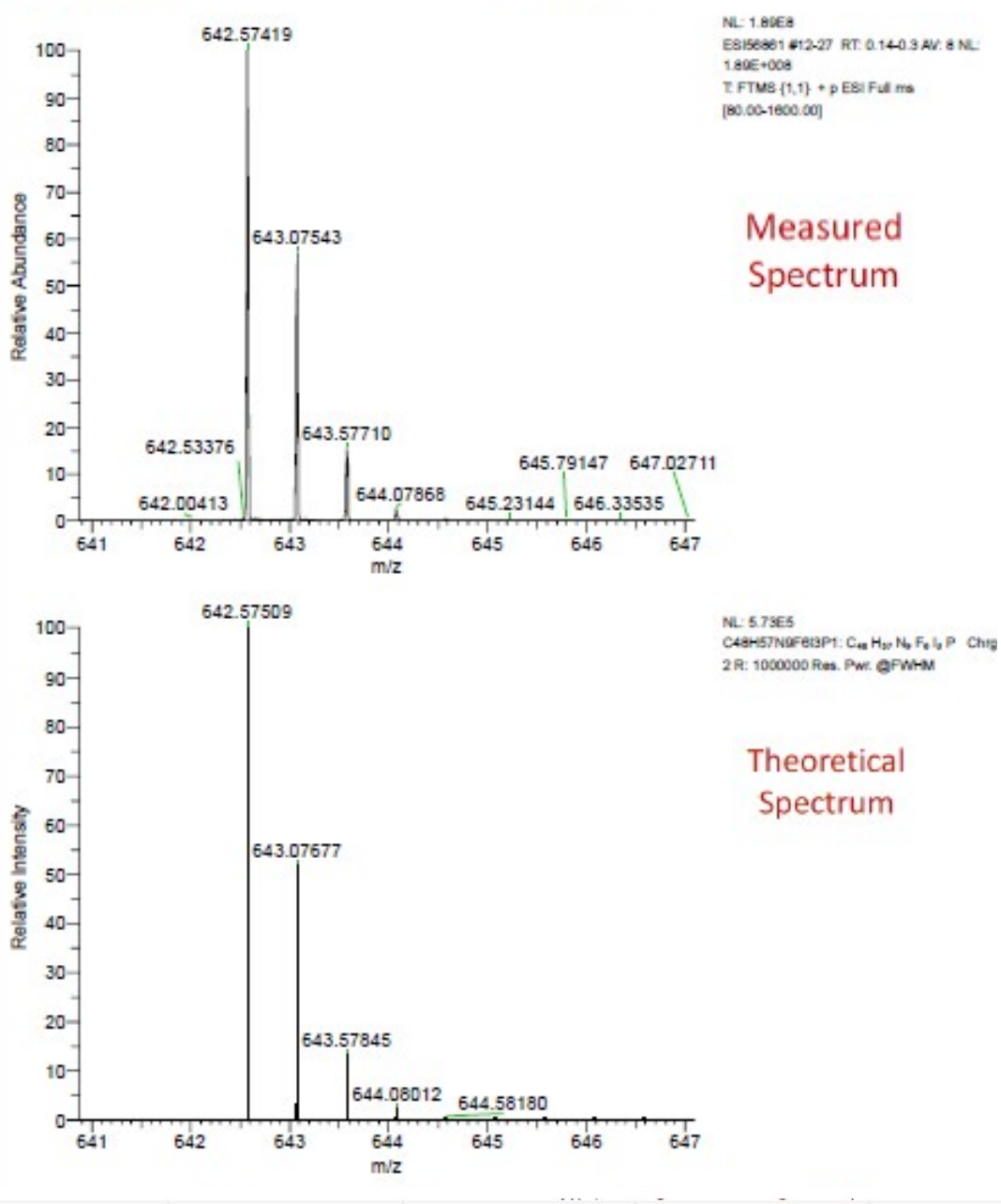

m/z	Formula	RDB	Delta ppm	Theo. Mass
642.57422	$C_{48}H_{57}N_9F_6{}^{127}I_3P$	21	-1.36	642.57509

Figure S16

S3. TITRATION EXPERIMENTS

The detection of various anions of tetrabutylammonium salts was determined by ^{1}HNMR spectroscopy in DMSO-d_6. The large downfield shifts of some protons of the imidazolium and triazolium rings suggest complexation between these hosts and anion (Cl^-, Br^-, I^-, $H_2PO_4^-$).

Titrations compound [2-H](PF_6)

a) Chloride titration

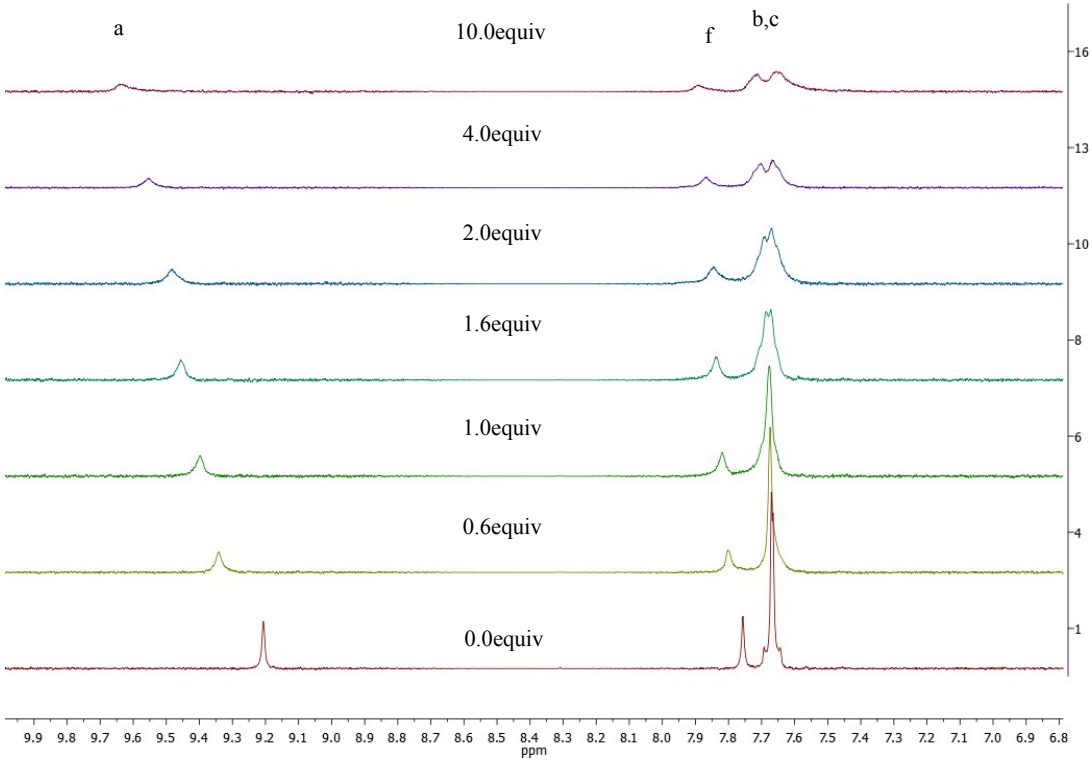

Figure S7.17. Partial ^{1}H NMR (400Hz) changes observed for the host [**2-H**](PF_6)in DMSO-d^6 during the addition of Cl^-

Table S7.1: Data values from the titration study of **[2-H](PF$_6$)**with Cl$^-$

[**2-H**](PF$_6$) (M)	**equiv NBu$_4$Cl**	**δa (ppm)**	**δf (ppm)**	**Δδa (ppm)**	**Δδf (ppm)**	**[NBu$_4$Cl] (M)**
0,002	0,0	9,2064	7,7565	0,0000	0,0000	0
0,001992	0,2	9,2639	7,7753	0,0575	0,0188	0,000398
0,001984	0,4	9,3100	7,7904	0,1036	0,0339	0,000794
0,001976	0,6	9,3417	7,8000	0,1353	0,0435	0,001186
0,001969	0,8	9,3676	7,8084	0,1612	0,0519	0,001575
0,001961	1,0	9,3982	7,8193	0,1918	0,0628	0,001961
0,001953	1,2	9,4233	7,8276	0,2169	0,0711	0,002344
0,001938	1,6	9,4558	7,8376	0,2494	0,0811	0,003101
0,001931	1,8	9,4674	7,8410	0,2610	0,0845	0,003475
0,001923	2,0	9,4821	7,8450	0,2757	0,0885	0,003846
0,001905	2,5	9,5067	7,8536	0,3003	0,0971	0,004762
0,001887	3,0	9,5248	7,8596	0,3184	0,1031	0,00566
0,001869	3,5	9,5540	7,8674	0,3476	0,1109	0,006542
0,001818	5,0	9,5760	7,8748	0,3696	0,1183	0,009091
0,001754	7,0	9,6044	7,8809	0,3980	0,1244	0,012281
0,001667	10,0	9,6300	7,8890	0,4236	0,1325	0,016667

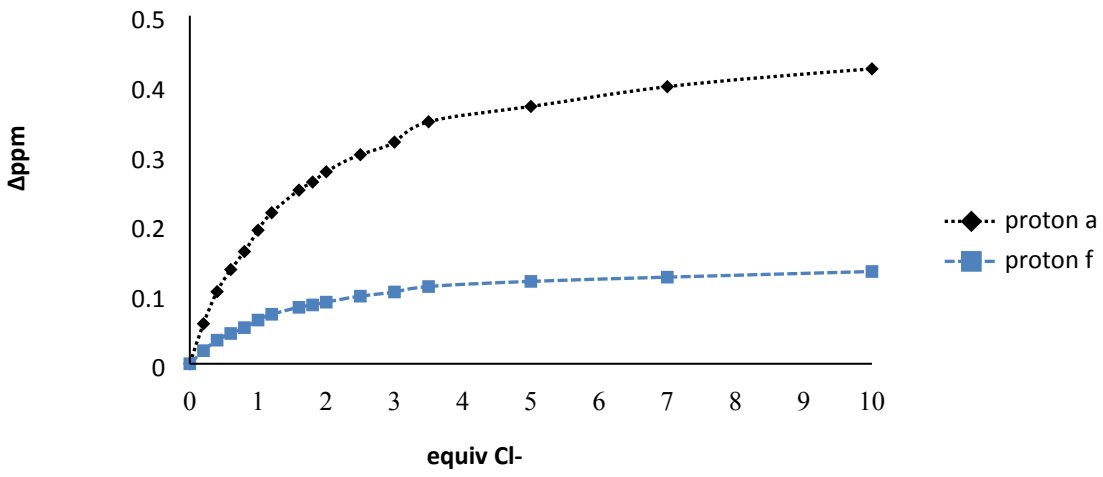

Figure S18. Plot of the data values from the titration study of [**2-H**](PF$_6$)with Cl$^-$

b) Bromide titration

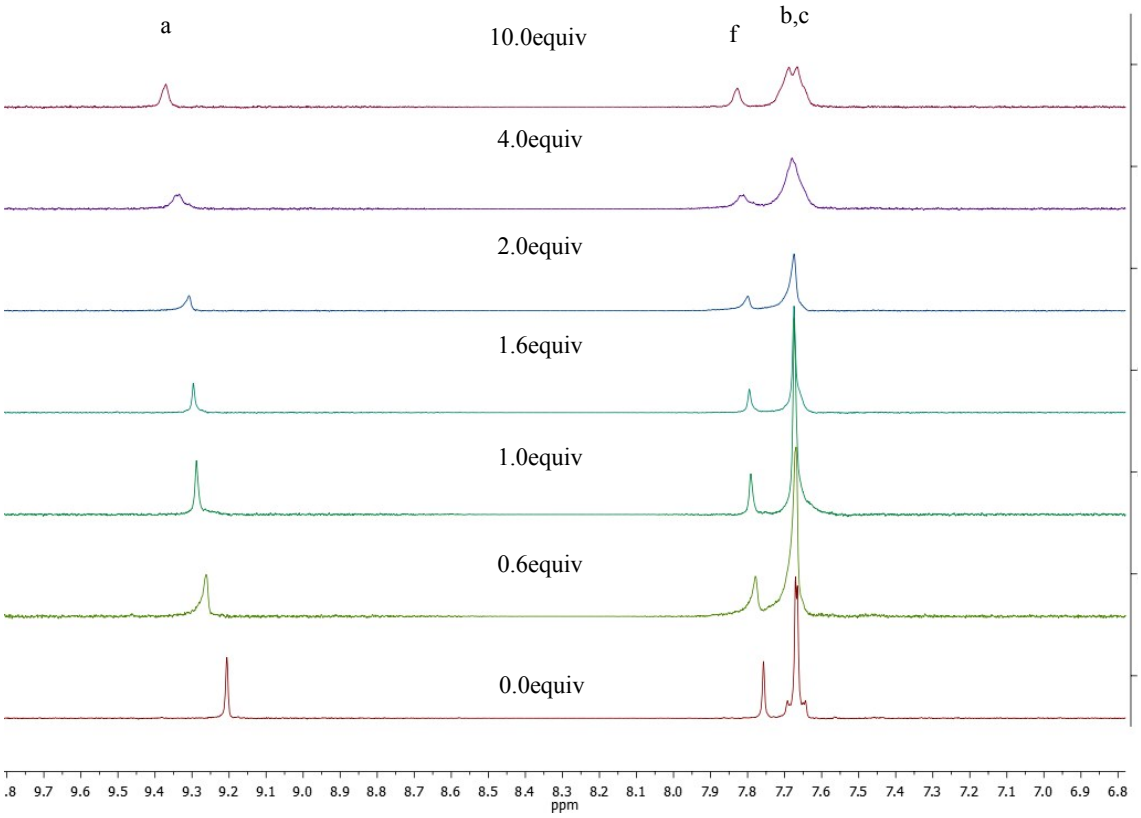

Figure S19. Partial ^{1}H NMR (400Hz) changes observed for the host [**2-H**](PF_6) in DMSO-d^6 during the addition of Br^-

Table S2: Data values from the titration study of **[2-**H**](PF$_6$)**with Br^-

[**2-H**](PF$_6$) (M)	**equiv NBu$_4$Br**	**δa (ppm)**	**δf (ppm)**	**δa (ppm)**	**Δδf (ppm)**	**[NBu$_4$Br] (M)**
0,002	0,0	9,2061	7,7569	0,0000	0	0
0,001992	0,2	9,2100	7,7606	0,0039	0,0037	0,000398
0,001984	0,4	9,2389	7,7703	0,03280	0,0134	0,000794
0,001976	0,6	9,2519	7,7749	0,0458	0,018	0,001186
0,001969	0,8	9,2623	7,7793	0,0562	0,0224	0,001575
0,001961	1,0	9,2719	7,7800	0,0658	0,0231	0,001961
0,001953	1,2	9,2787	7,7809	0,0726	0,02399	0,002344
0,001946	1,4	9,2879	7,7911	0,0818	0,0342	0,002724
0,001938	1,6	9,2962	7,7951	0,0901	0,0382	0,003101
0,001931	1,8	9,2999	7,7961	0,0938	0,0392	0,003475
0,001923	2,0	9,3091	7,8003	0,1030	0,0434	0,003846
0,001905	2,5	9,3158	7,8041	0,1097	0,0472	0,004762
0,001887	3,0	9,3232	7,8074	0,1171	0,0505	0,00566
0,001869	3,5	9,3368	7,8152	0,1307	0,0583	0,006542
0,001818	5,0	9,3455	7,8172	0,1394	0,0603	0,009091
0,001754	7,0	9,3606	7,8241	0,1545	0,0672	0,012281
0,001667	10,0	9,3718	7,8289	0,1657	0,072	0,016667

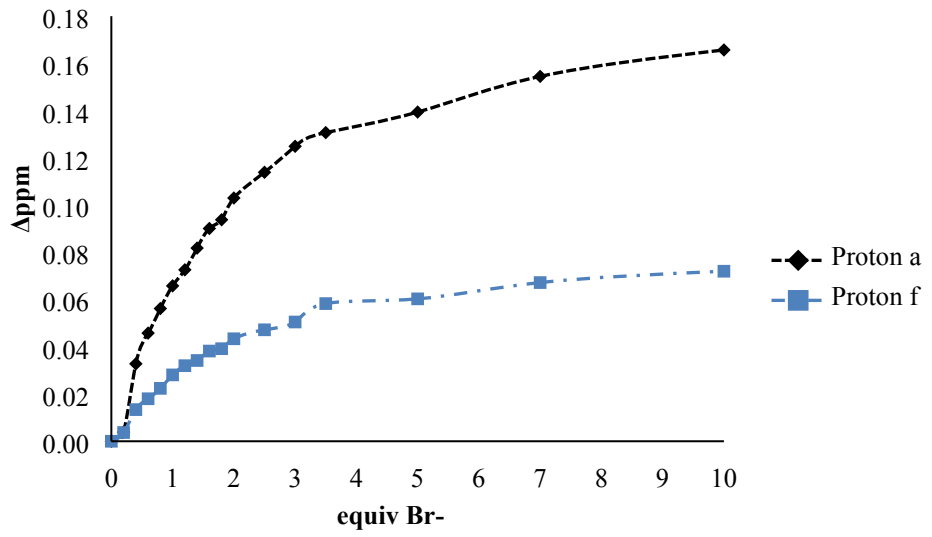

Figure S20. Plot of the data values from the titration study of [**2-H**](PF_6)with Br^-

c) Iodide titration

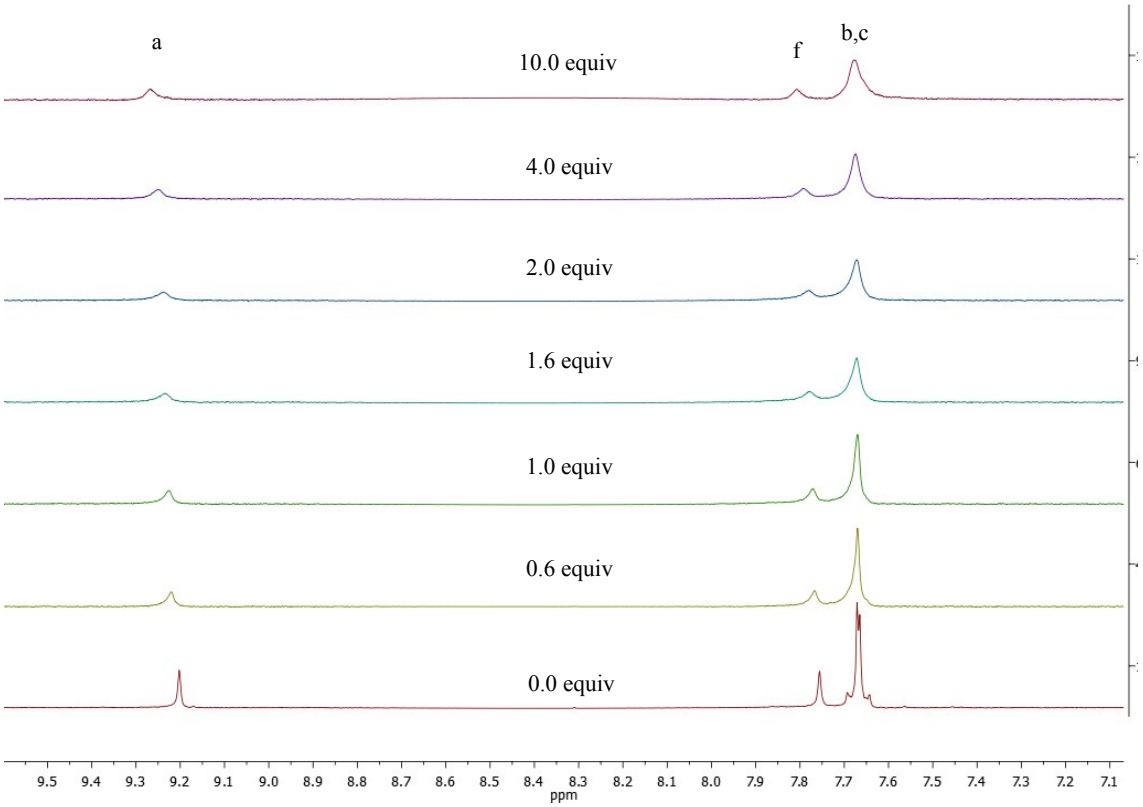

Figure S21. Partial ^{1}H NMR (400Hz) changes observed for the host [**2-H**](PF_6)in DMSO-d^6 during the addition of I^-

Table S3: Data values from the titration study of **19(PF$_6$)$_3$** with I$^-$

[**2-H**](PF$_6$) (M)	**equiv NBu$_4$I**	**δa (ppm)**	**δf (ppm)**	**δa (ppm)**	**Δδf (ppm)**	**[NBu$_4$I] (M)**
0,002	0,0	9,2023	7,755900	0,0000	0,0000	0
0,001992	0,2	9,2090	7,759300	0,0067	0,0034	0,000398
0,001984	0,4	9,2151	7,762700	0,0128	0,0068	0,000794
0,001976	0,6	9,2210	7,767400	0,0187	0,0115	0,001186
0,001969	0,8	9,2225	7,768700	0,0202	0,0128	0,001575
0,001961	1,0	9,2268	7,771700	0,0245	0,0158	0,001961
0,001953	1,2	9,2309	7,775800	0,0286	0,0199	0,002344
0,001946	1,4	9,2336	7,776900	0,0313	0,0210	0,002724
0,001938	1,6	9,2359	7,779000	0,0336	0,0231	0,003101
0,001931	1,8	9,2359	7,780200	0,0336	0,0243	0,003475
0,001923	2,0	9,2408	7,781300	0,0385	0,0254	0,003846
0,001905	2,5	9,2433	7,785400	0,0410	0,0295	0,004762
0,001887	3,0	9,2483	7,788900	0,0460	0,0330	0,00566
0,001869	3,5	9,2506	7,792700	0,0483	0,0368	0,006542
0,001818	5,0	9,2532	7,796000	0,0509	0,0401	0,009091
0,001754	7,0	9,2575	7,802300	0,0552	0,0464	0,012281
0,001667	10,0	9,2600	7,80600	0,0577	0,0501	0,016667

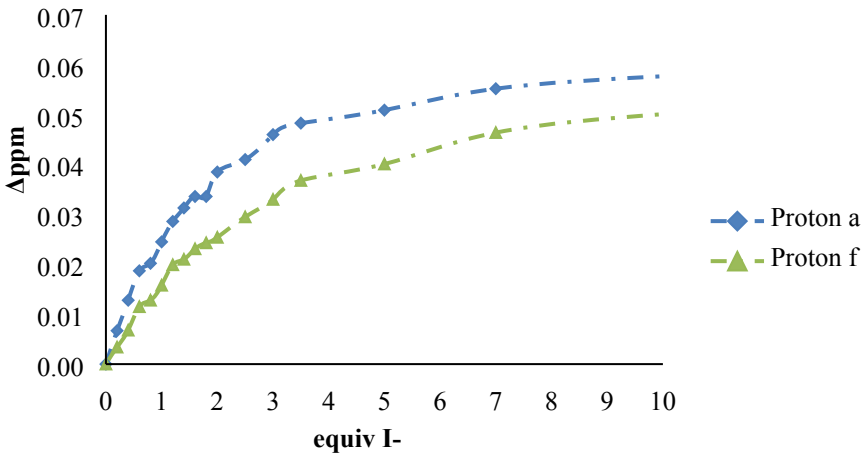

Figure S22. Plot of the data values from the titration study of [**2-H**](PF$_6$)with I$^-$

d) Dihydrogen phospahate titration

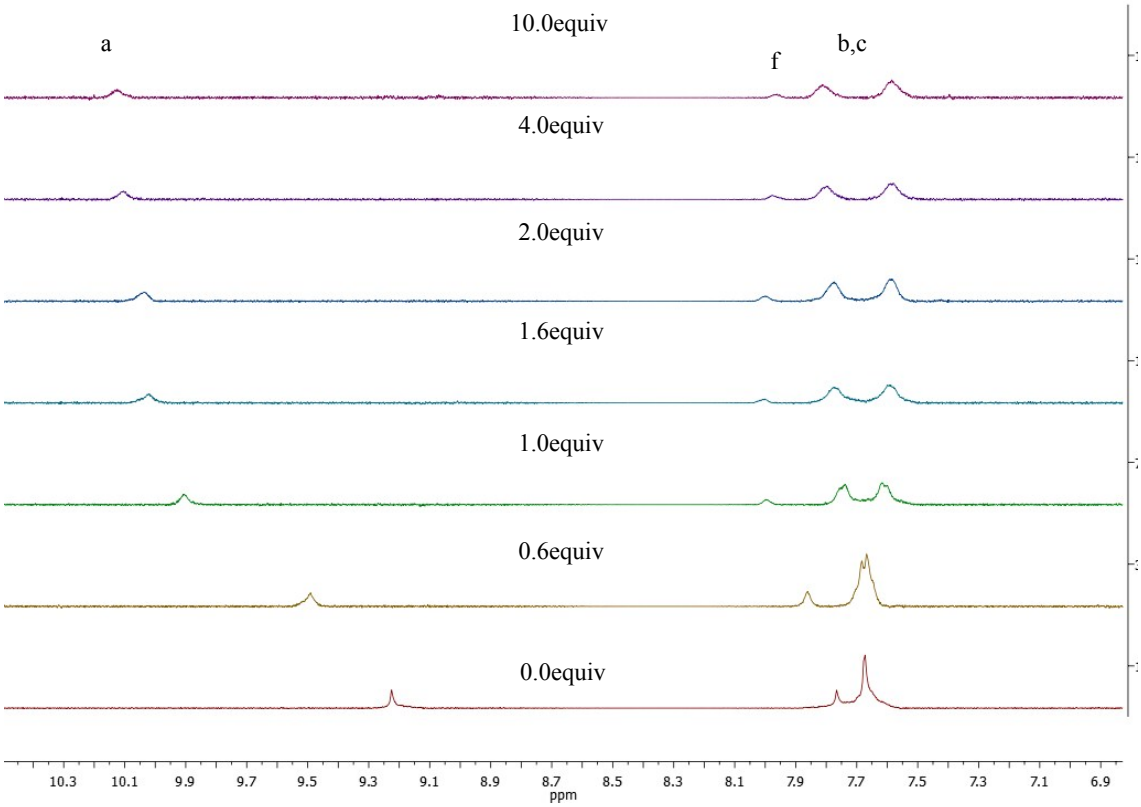

Figure S23. Partial ^{1}H NMR (400Hz) changes observed for the host [**2-H**](PF_6)in DMSO-d^6 during the addition of $H_2PO_4^-$

Table S4: Data values from the titration study of **[2-H](PF$_6$)** with I^-

[**2-H**](PF$_6$) (M)	**equiv** $NBu_4H_2PO_4$	**δa** (ppm)	**Δδa** (ppm)	**[$NBu_4H_2PO_4$]** (M)
0,002	0,0	9,2242	0	0
0,001992	0,2	9,3530	0,1288	0,000398
0,001984	0,4	9,4915	0,2673	0,000794
0,001976	0,6	9,6040	0,3798	0,001186
0,001969	0,8	9,7275	0,5033	0,001575
0,001961	1,0	9,8372	0,613	0,001961
0,001953	1,2	9,9052	0,681	0,002344
0,001946	1,4	9,9583	0,7341	0,002724
0,001938	1,6	9,9854	0,7612	0,003101
0,001931	1,8	10,0221	0,7979	0,003475
0,001923	2,0	10,0380	0,8138	0,003846
0,001905	2,5	10,0571	0,8329	0,004762
0,001887	3,0	10,0841	0,8599	0,00566
0,001869	3,5	10,1049	0,8807	0,006542
0,001818	5,0	10,1196	0,8954	0,009091
0,001754	7,0	10,1245	0,9003	0,012281
0,001667	10,0	10,1300	0,9058	0,016667

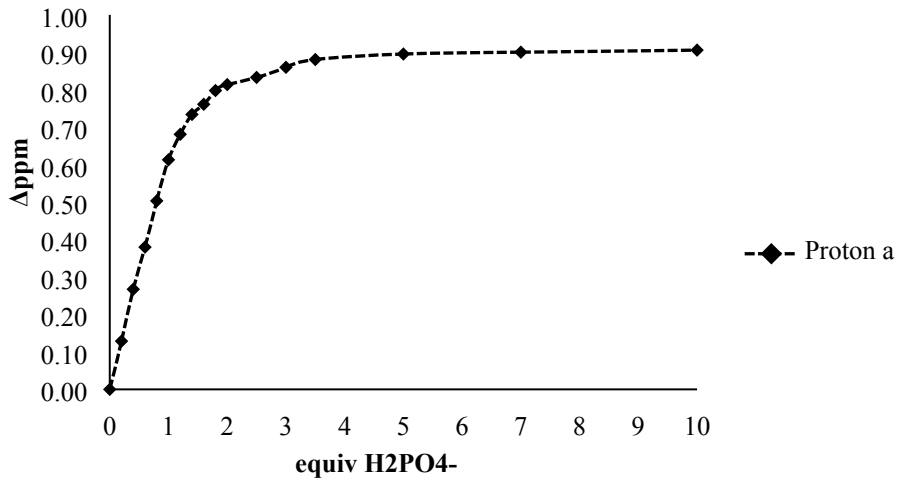

Figure S24. Plot of the data values from the titration study of [**2-H**](PF$_6$)with $H_2PO_4^-$

Titrations compound 20(PF$_6$)$_3$

a) Chloride titration

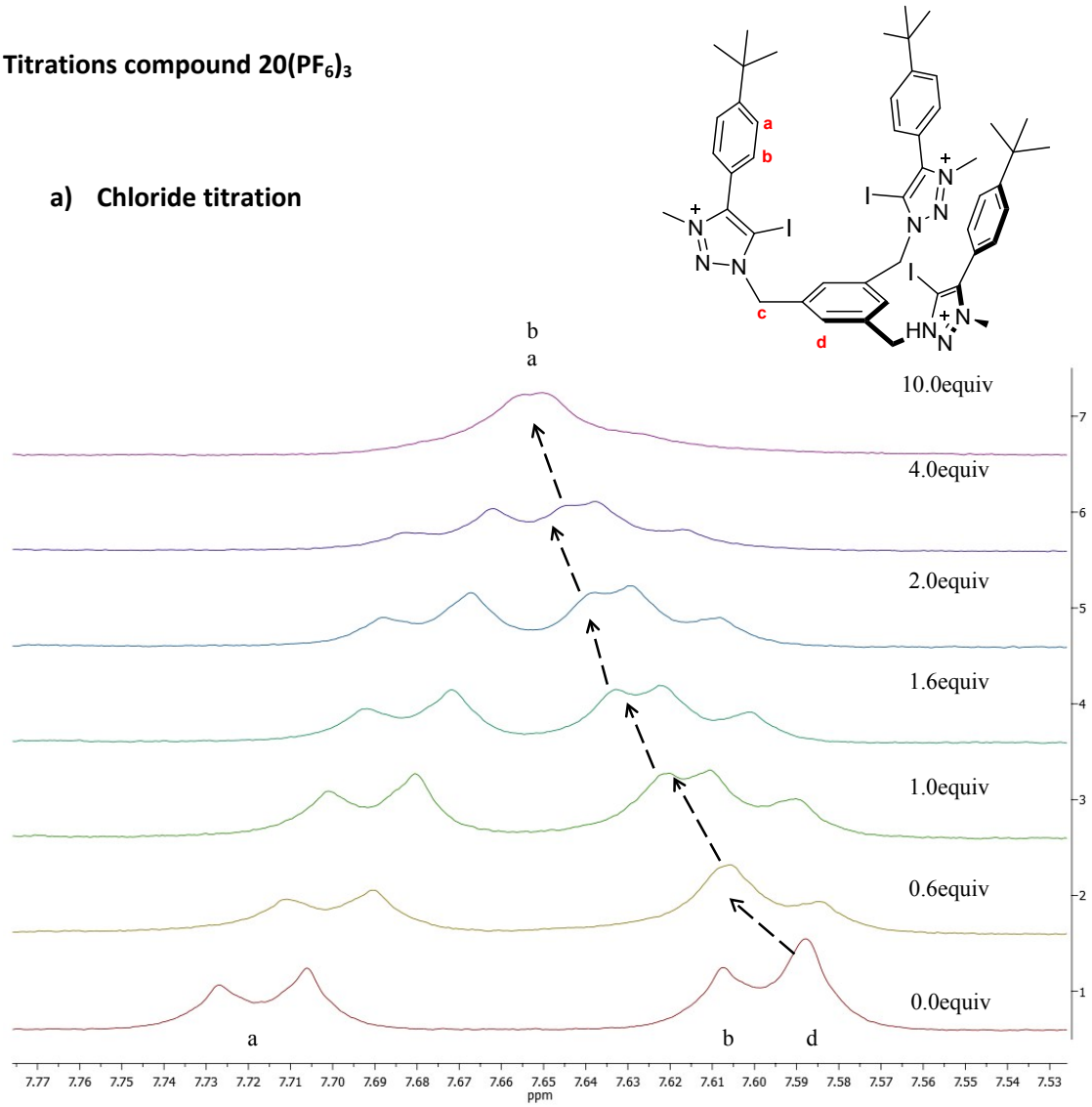

Figure S25. Partial ^{1}H NMR (400Hz) changes observed for the host [**2-I**](PF$_6$) in DMSO-d^6 during the addition of Cl^-

Table S5: Data values from the titration study of **20(PF$_6$)$_3$** with Cl$^-$

[**2-I**](PF$_6$) (M)	equiv NBu4Cl	δa (ppm)	δb (ppm)	δd (ppm)	Δδa (ppm)	Δδb (ppm)	Δδd (ppm)	[NBu$_4$Cl] (M)
2,00E-03	0,0	7,7273	7,7073	7,5887	0	0	0	1,00E-11
0,001992032	0,2	7,7214	7,7012	7,5969	-0,0059	-0,0061	0,0082	0,0003984
0,001984127	0,4	7,7168	7,6964	7,6045	-0,0105	-0,0109	0,0158	0,0007937
0,001976285	0,6	7,7112	7,6909	7,6067	-0,0161	-0,0164	0,018	0,0011858
0,001968504	0,8	7,7096	7,6893	7,612	-0,0177	-0,018	0,0233	0,0015748
0,001960784	1,0	7,7039	7,6839	7,6182	-0,0234	-0,0234	0,0295	0,0019608
0,001953125	1,2	7,7007	7,6806	7,6216	-0,0266	-0,0267	0,0329	0,0023438
0,001945525	1,4	7,6954	7,6758	7,6257	-0,0319	-0,0315	0,037	0,0027237
0,001937984	1,6	7,6939	7,6737	7,6299	-0,0334	-0,0336	0,0412	0,0031008
0,001930502	1,8	7,692	7,6721	7,6333	-0,0353	-0,0352	0,0446	0,0034749
0,001923077	2,0	7,6901	7,6704	7,635	-0,0372	-0,0369	0,0463	0,0038462
0,001904762	2,5	7,6878	7,6677	7,638	-0,0395	-0,0396	0,0493	0,0047619
0,001886792	3,0	7,6858	7,6653	7,641	-0,0415	-0,042	0,0523	0,0056604
0,001869159	3,5	7,6826	7,6629	7,644	-0,0447	-0,0444	0,0553	0,0065421
0,001818182	5,0	7,6803	7,6606	7,647	-0,047	-0,0467	0,0583	0,0090909
0,001754386	10,0	7,68	7,6606	7,65	-0,0473	-0,0467	0,0613	0,0122807

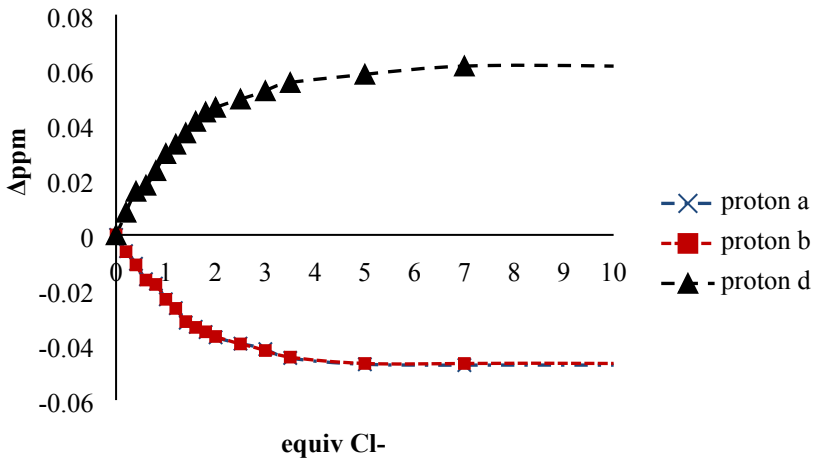

Figure S26. Plot of the data values from the titration study of [**2-I**](PF$_6$) with Cl$^-$

b) Bromide titration

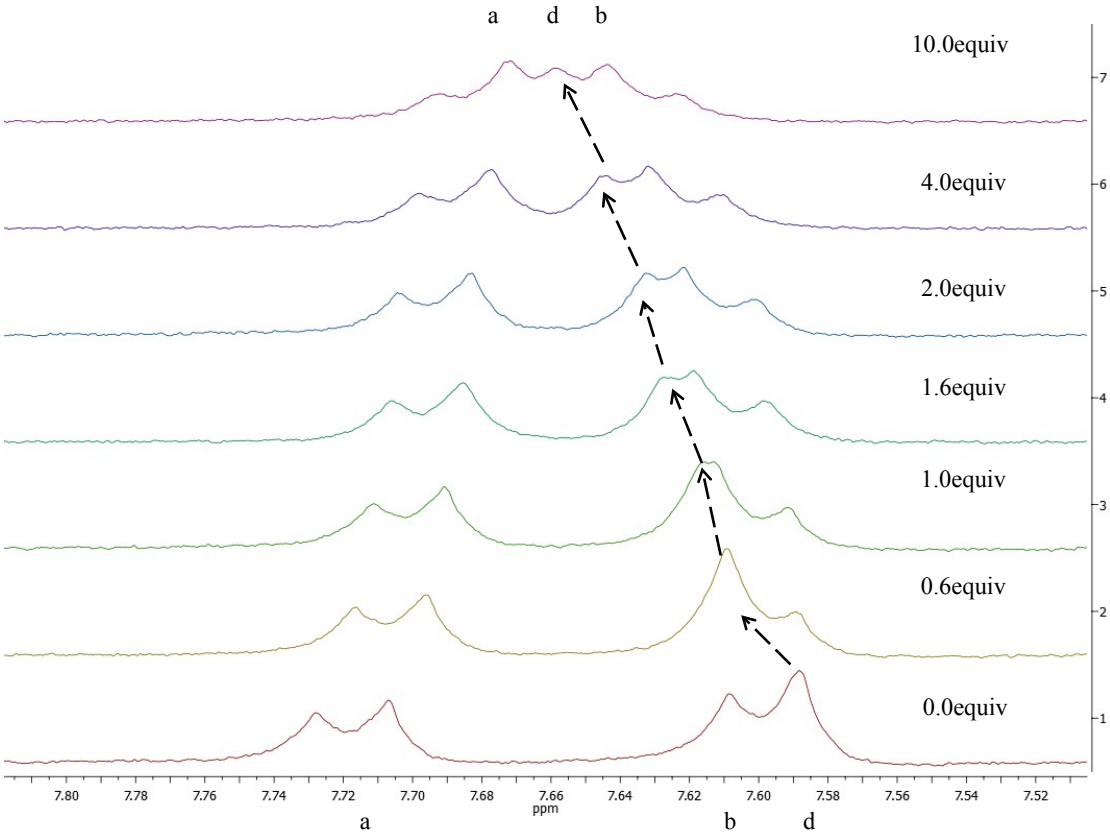

Figure S27. Partial ^{1}H NMR (400Hz) changes observed for the host [**2-I**](PF_6) in DMSO-d^6 during the addition of Br^-

Table S6: Data values from the titration study of **[2-I](PF$_6$)** with Br$^-$

[2-I](PF6) (M)	equiv NBu4Cl	δa (ppm)	δb (ppm)	δd (ppm)	Δδa (ppm)	Δδb (ppm)	Δδd (ppm)	[NBu$_4$Cl] (M)
0,002000	0,0	7,7272	7,7073	7,5882	0	0	0	0,000000
0,001992	0,2	7,7234	7,7035	7,5936	-0,0038	-0,0038	0,0054	0,000398
0,001984	0,4	7,7197	7,6997	7,6	-0,0075	-0,0076	0,0118	0,000794
0,001976	0,6	7,716	7,6963	7,6087	-0,0112	-0,011	0,0205	0,001186
0,001969	0,8	7,7143	7,6941	7,6119	-0,0129	-0,0132	0,0237	0,001575
0,001961	1,0	7,7119	7,6919	7,6172	-0,0153	-0,0154	0,029	0,001961
0,001953	1,2	7,7099	7,6897	7,622	-0,0173	-0,0176	0,0338	0,002344
0,001946	1,4	7,7069	7,6871	7,625	-0,0203	-0,0202	0,0368	0,002724
0,001938	1,6	7,706	7,6857	7,6279	-0,0212	-0,0216	0,0397	0,003101
0,001931	1,8	7,705	7,6847	7,63	-0,0222	-0,0226	0,0418	0,003475
0,001923	2,0	7,7034	7,6833	7,6321	-0,0238	-0,024	0,0439	0,003846
0,001905	2,5	7,7018	7,6818	7,6367	-0,0254	-0,0255	0,0485	0,004762
0,001887	3,0	7,7004	7,68	7,6397	-0,0268	-0,0273	0,0515	0,005660
0,001869	3,5	7,6979	7,6776	7,6449	-0,0293	-0,0297	0,0567	0,006542
0,001818	5,0	7,6968	7,6763	7,6488	-0,0304	-0,031	0,062	0,009091
0,001754	7,0	7,6935	7,67441	7,6536	-0,0337	-0,03289	0,067	0,012281
0,001667	10	7,6921	7,6722	7,657	-0,0351	-0,0351	0,0688	0,016667

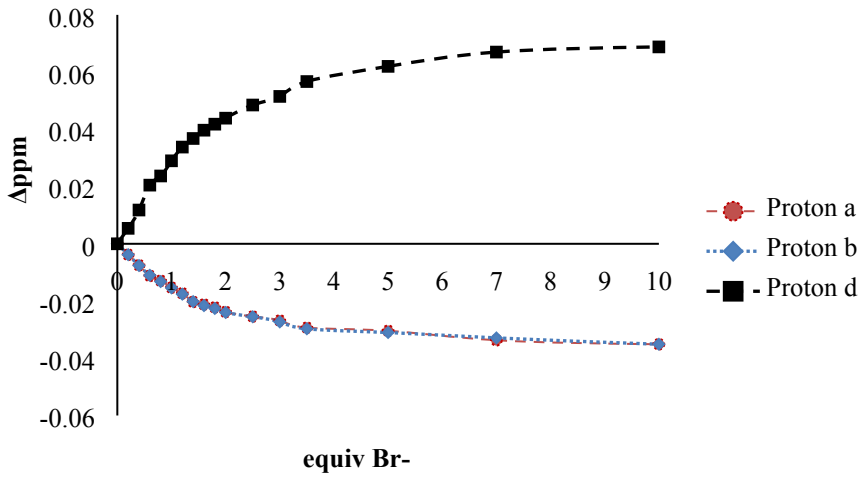

Figure S28. Plot of the data values from the titration study of [**2-I**](PF$_6$) with Br$^-$

c) Iodide titration

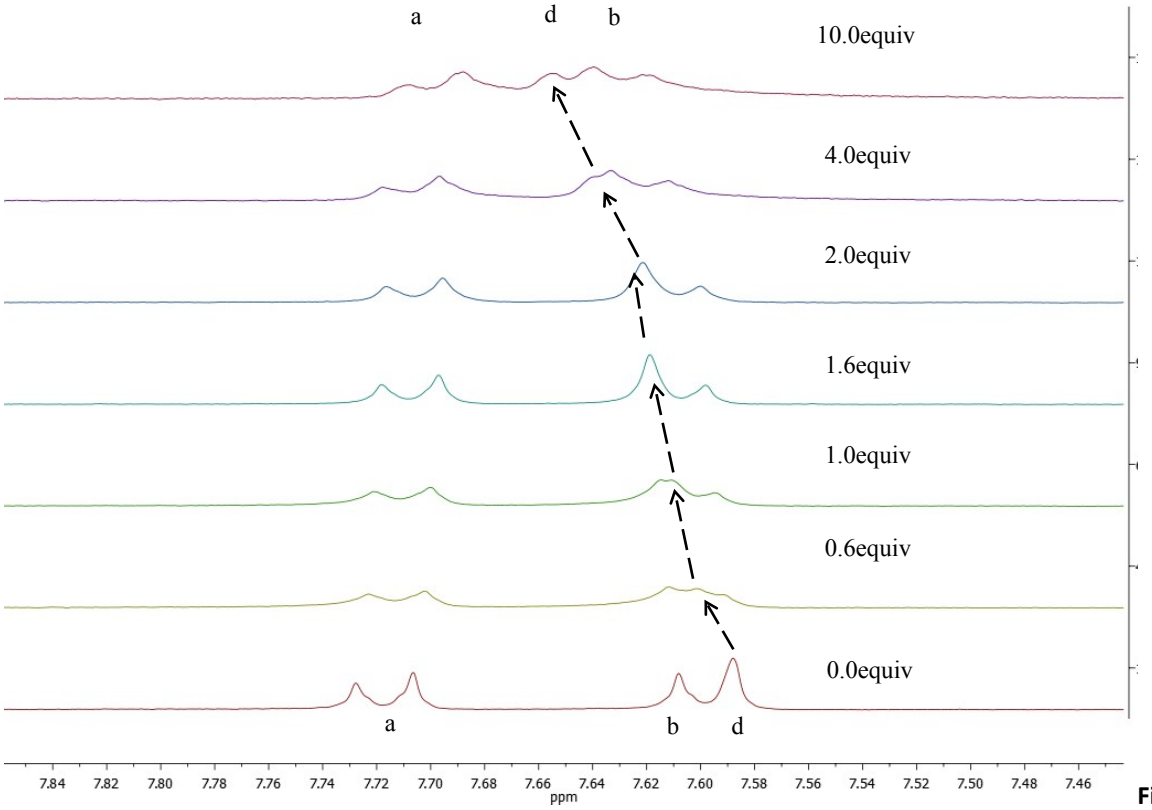

Figure S29. Partial ^{1}H NMR (400Hz) changes observed for the host [**2-I**](PF_6) in DMSO-d^6 during the addition of I^-

Table S7: Data values from the titration study of **[2-I](PF$_6$)** with I$^-$

[2-I](PF6) (M)	equiv NBu4I	δa (ppm)	Δδa (ppm)	[NBu$_4$I] (M)
0,002	0,0	7,5883	0	0
0,001992	0,2	7,5911	0,0028	0,000398
0,001984	0,4	7,5931	0,0048	0,000794
0,001976	0,6	7,6011	0,0128	0,001186
0,001969	0,8	7,6049	0,0166	0,001575
0,001961	1,0	7,6096	0,0213	0,001961
0,001953	1,2	7,6128	0,0245	0,002344
0,001946	1,4	7,6176	0,0293	0,002724
0,001938	1,6	7,6187	0,0304	0,003101
0,001931	1,8	7,621	0,0327	0,003475
0,001923	2,0	7,6212	0,0329	0,003846
0,001905	2,5	7,6238	0,0355	0,004762
0,001887	3,0	7,6264	0,0381	0,00566
0,001869	3,5	7,6285	0,0402	0,006542
0,001818	5,0	7,6315	0,0432	0,009091
0,001754	7,0	7,6335	0,0452	0,012281
0,001667	10,0	7,638	0,05	0,016667

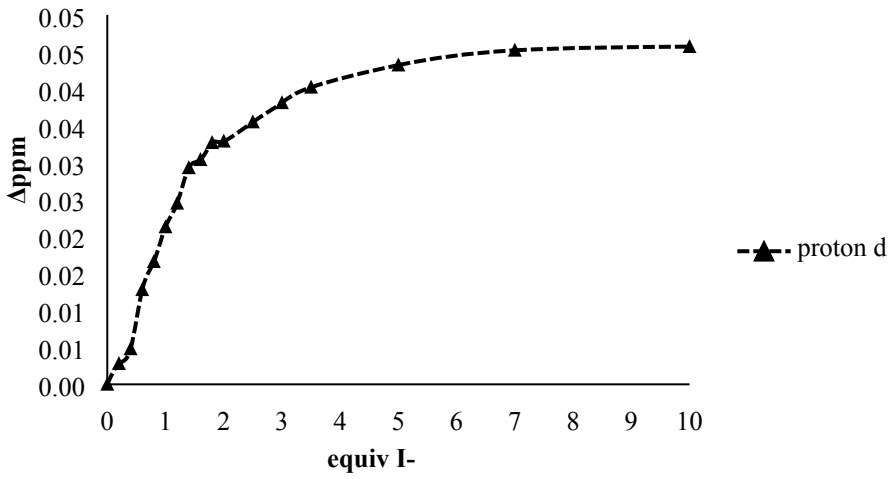

Figure S30. Plot of the data values from the titration study of [**2-I**](PF$_6$) with I$^-$

d) Dihydrogen phospate titration

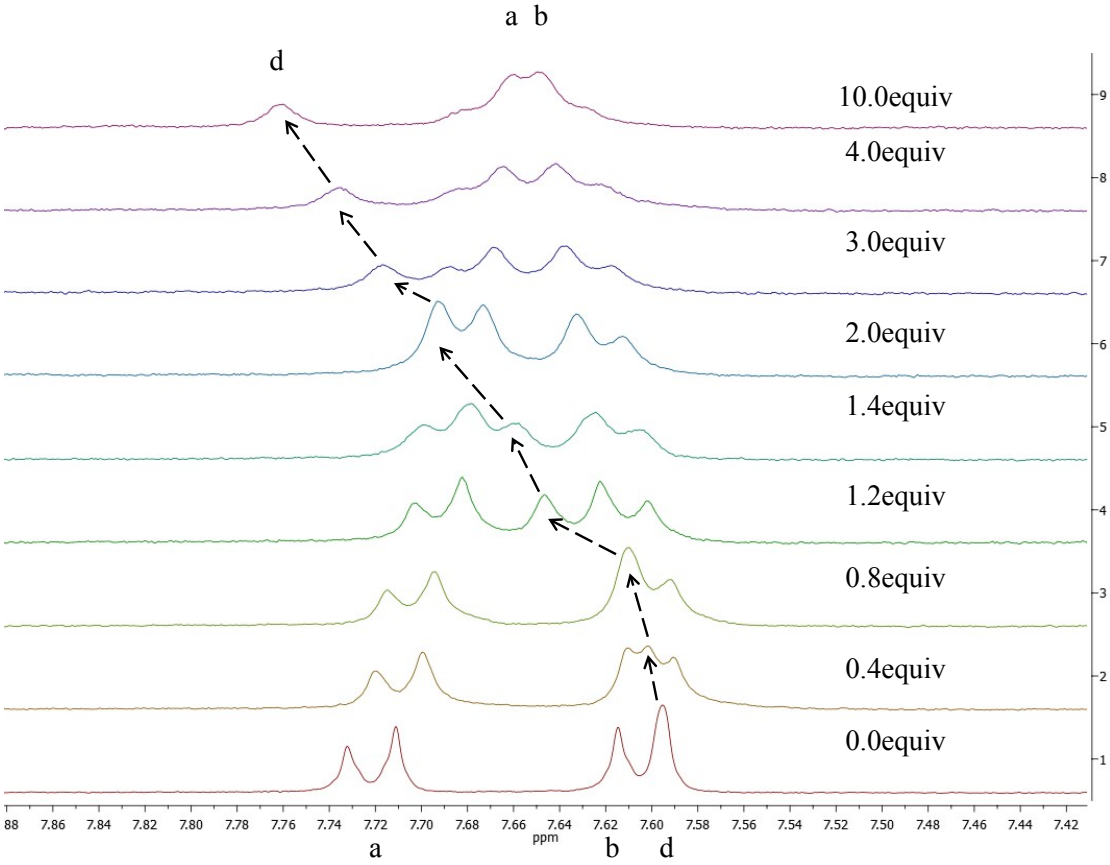

Figure S31. Partial ^{1}H NMR (400Hz) changes observed for the host [**2-I**](PF_6) in DMSO-d^6 during the addition of $H_2PO_4^-$

Table S8: Data values from the titration study of **20(PF$_6$)$_3$** with $H_2PO_4^-$

[2-I](PF6) (M)	equiv $NBu_4H_2PO_4$	δd (ppm)	Δδd (ppm)	[$NBu_4H_2PO_4$] (M)
0,002	0,0	7,59	0	0
0,001992	0,2	7,61	0,02	0,000398
0,001984	0,4	7,626	0,036	0,000794
0,001976	0,6	7,639	0,049	0,001186
0,001969	0,8	7,65	0,06	0,001575
0,001961	1,0	7,659	0,069	0,001961
0,001953	1,2	7,67	0,08	0,002344
0,001946	1,4	7,679	0,089	0,002724
0,001938	1,6	7,689	0,099	0,003101
0,001931	1,8	7,696	0,106	0,003475
0,001923	2,0	7,71	0,12	0,003846
0,001905	2,5	7,72	0,13	0,004762
0,001887	3,0	7,73	0,14	0,00566
0,001869	3,5	7,735	0,145	0,006542
0,001818	5,0	7,747	0,157	0,009091
0,001754	7,0	7,752	0,162	0,012281
0,001667	10,0	7,757	0,167	0,016667

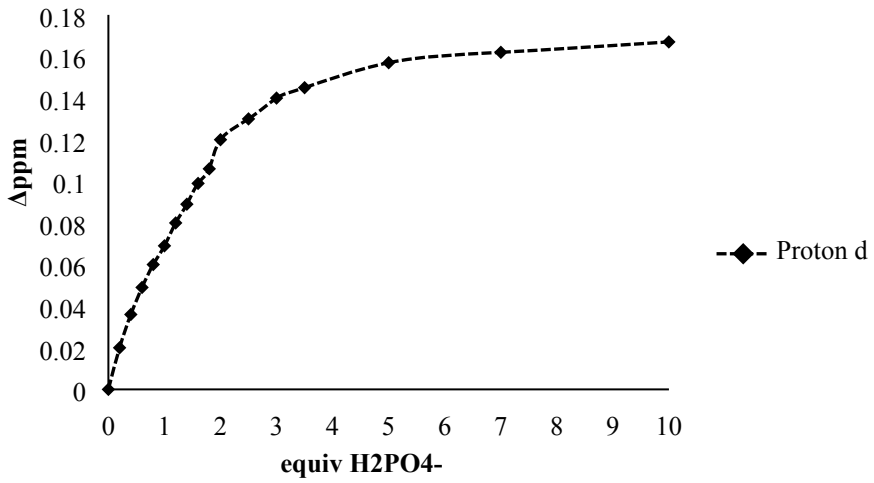

Figure S32. Plot of the data values from the titration study of [**2-I**](PF$_6$) with $H_2PO_4^-$

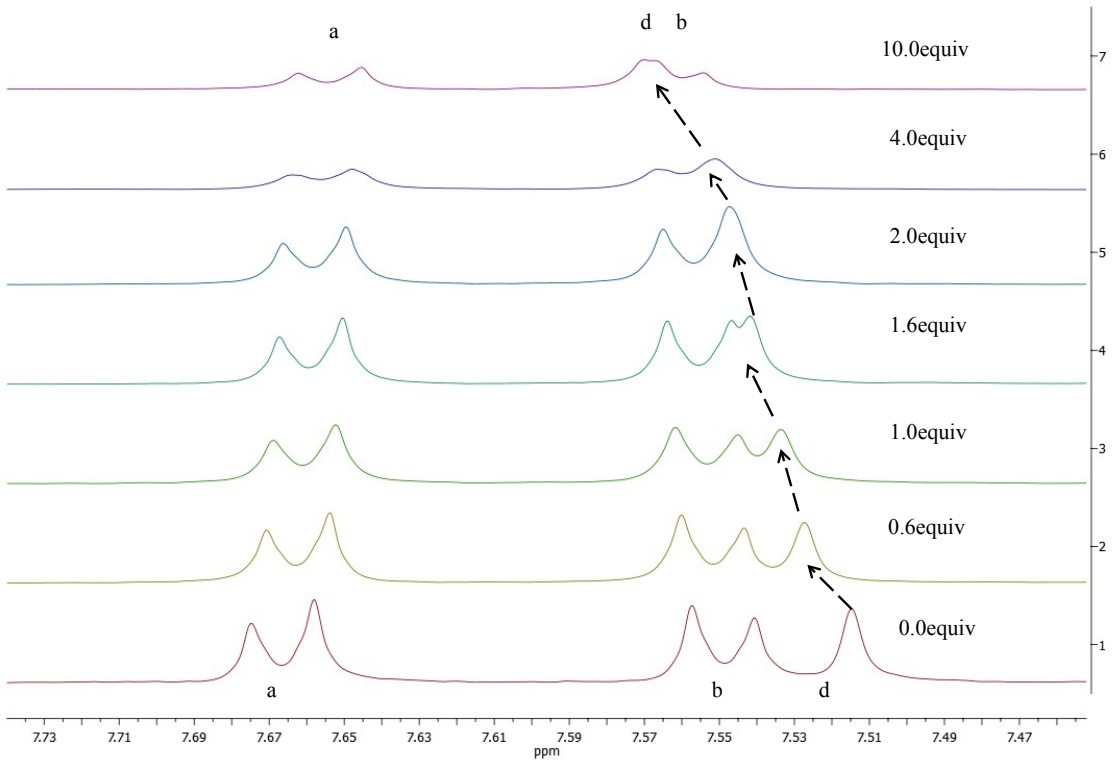

Figure S33. Partial ^{1}H NMR (400Hz) changes observed for the host [**2-I**](PF_6) DMSO-d^6: D_2O during the addition of $H_2PO_4^-$

Table S9: Data values from the titration study of [**2-I**](PF_6) with $H_2PO_4^-$ (DMSO-d^6: D_2O)

[2-I](PF6) (M)	equiv $NBu_4H_2PO_4$	δd (ppm)	Δδd (ppm)	[$NBu_4H_2PO_4$] (M)
0,002	0,0	7,5146	0	0
0,001992	0,2	7,5195	0,0049	0,000398
0,001984	0,4	7,5228	0,0082	0,000794
0,001976	0,6	7,5275	0,0129	0,001186
0,001969	0,8	7,5302	0,0156	0,001575
0,001961	1,0	7,5338	0,0192	0,001961
0,001953	1,2	7,5363	0,0217	0,002344
0,001946	1,4	7,5392	0,0246	0,002724
0,001938	1,6	7,5421	0,0275	0,003101
0,001931	1,8	7,5445	0,0299	0,003475
0,001923	2,0	7,546	0,0314	0,003846
0,001905	2,5	7,549	0,0344	0,004762
0,001887	3,0	7,5512	0,0366	0,00566
0,001869	3,5	7,5535	0,0389	0,006542
0,001818	5,0	7,557	0,0424	0,009091
0,001754	7,0	7,561	0,0464	0,012281
0,001667	10,0	7,566	0,05	0,016667

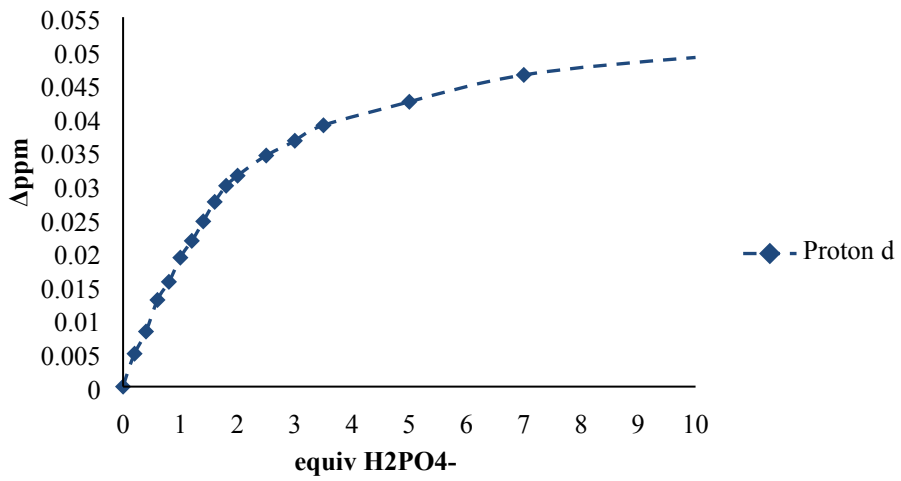

Figure S34: Plot of the data values from the titration study of [**2-I**](PF_6) with $H_2PO_4^-$ (DMSO-d^6: D_2O)

Titrations compound [**1-H**](PF_6)

a) Chloride titration

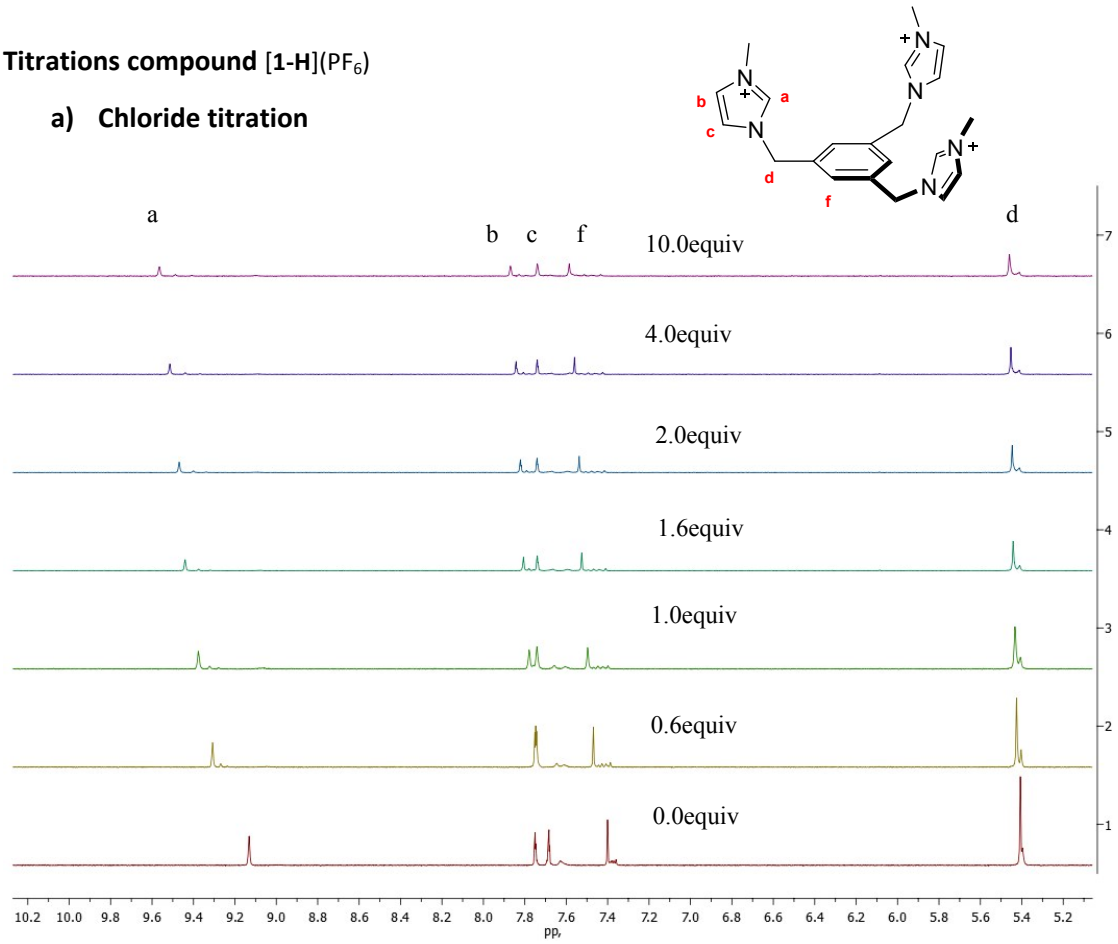

Figure S35. Partial ^{1}H NMR (400Hz) changes observed for the host [**1-H**](PF_6)in DMSO-d^6 during the addition of Cl^-

Table S10: Data values from the titration study of **[1-H](PF$_6$)**with Cl$^-$

[1-H](PF$_6$) (M)	equiv NBu$_4$Cl	δa (ppm)	δf (ppm)	δd (ppm)	Δδa (ppm)	Δδf (ppm)	Δδd (ppm)	[NBu$_4$Cl] (M)
0,002	0,0	9,1310	7,400000	5,407	0	0	0	0
0,001992	0,2	9,2000	7,426000	5,414	0,069	0,026	0,007	0,000398
0,001984	0,4	9,2610	7,451000	5,421	0,13	0,051	0,014	0,000794
0,001976	0,6	9,3080	7,469000	5,426	0,177	0,069	0,019	0,001186
0,001969	0,8	9,3450	7,483000	5,43	0,214	0,083	0,023	0,001575
0,001961	1,0	9,3770	7,497000	5,433	0,246	0,097	0,026	0,001961
0,001953	1,2	9,4020	7,508000	5,436	0,271	0,108	0,029	0,002344
0,001946	1,4	9,4230	7,518000	5,439	0,292	0,118	0,032	0,002724
0,001938	1,6	9,4400	7,525000	5,442	0,309	0,125	0,035	0,003101
0,001931	1,8	9,4560	7,531000	5,444	0,325	0,131	0,037	0,003475
0,001923	2,0	9,4690	7,538000	5,446	0,338	0,138	0,039	0,003846
0,001905	2,5	9,4850	7,546000	5,449	0,354	0,146	0,042	0,004762
0,001887	3,0	9,4980	7,551000	5,45	0,367	0,151	0,043	0,00566
0,001869	3,5	9,5150	7,560000	5,453	0,384	0,16	0,046	0,006542
0,001818	5,0	9,5260	7,566000	5,454	0,395	0,166	0,047	0,009091
0,001754	7,0	9,5460	7,575000	5,457	0,415	0,175	0,05	0,012281
0,001667	10,0	9,5650	7,586000	5,46	0,434	0,186	0,053	0,016667

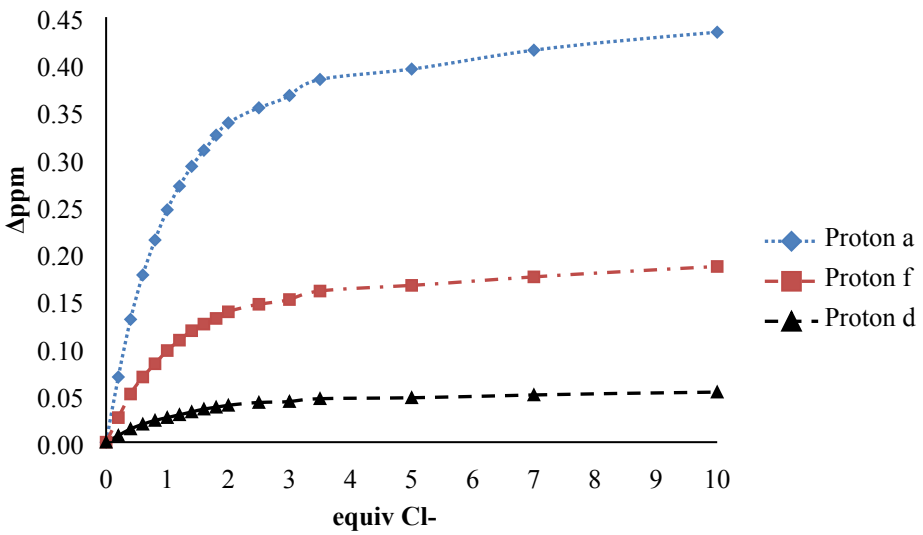

Figure S36. Plot of the data values from the titration study of [**1-H**](PF$_6$)with Cl$^-$

b) Bromide titration

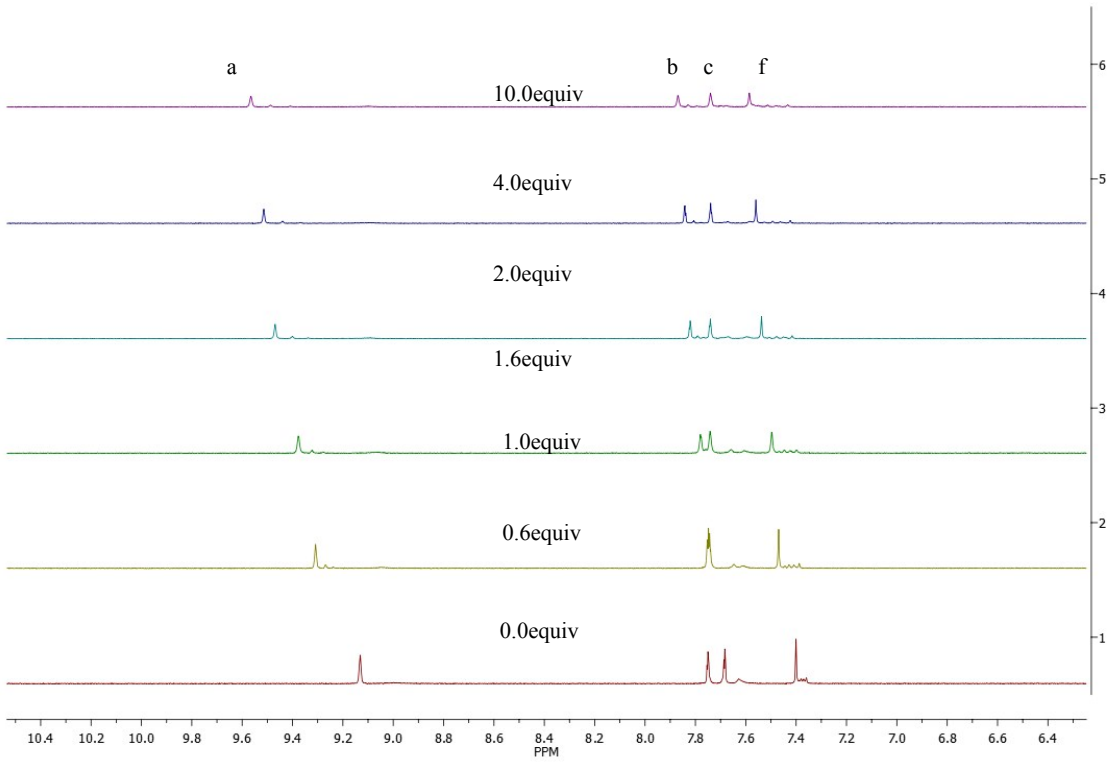

Figure S37. Partial ^{1}H NMR (400Hz) changes observed for the host [**1-H**](PF_6)in DMSO-d^6 during the addition of Br^-

Table S11: Data values from the titration study of **[1-H](PF$_6$)**with Br$^-$

[1-H](PF$_6$) (M)	equiv NBu4Br	δa (ppm)	δf (ppm)	δd (ppm)	Δδa (ppm)	Δδf (ppm)	Δδd (ppm)	[NBu$_4$Br] (M)
0,002	0,0	9,131	7,399	5,406	0	0	0	0
0,001992	0,2	9,168	7,418	5,414	0,037	0,019	0,008	0,000398
0,001984	0,4	9,193	7,433	5,420	0,062	0,034	0,014	0,000794
0,001976	0,6	9,214	7,443	5,425	0,083	0,044	0,019	0,001186
0,001969	0,8	9,231	7,452	5,429	0,1	0,053	0,023	0,001575
0,001961	1,0	9,245	7,460	5,432	0,114	0,061	0,026	0,001961
0,001953	1,2	9,258	7,468	5,434	0,127	0,069	0,028	0,002344
0,001946	1,4	9,268	7,474	5,437	0,137	0,075	0,031	0,002724
0,001938	1,6	9,2780	7,480	5,440	0,147	0,081	0,034	0,003101
0,001931	1,8	9,287	7,484	5,442	0,156	0,085	0,036	0,003475
0,001923	2,0	9,291	7,485	5,445	0,16	0,086	0,039	0,003846
0,001905	2,5	9,303	7,495	5,447	0,172	0,096	0,041	0,004762
0,001887	3,0	9,311	7,500	5,449	0,18	0,101	0,043	0,00566
0,001869	3,5	9,3210	7,505	5,451	0,19	0,106	0,045	0,006542
0,001818	5,0	9,330	7,511	5,454	0,199	0,112	0,048	0,009091
0,001754	7,0	9,343	7,518	5,456	0,212	0,119	0,05	0,012281
0,001667	10,0	9,358	7,527	5,461	0,227	0,128	0,055	0,016667

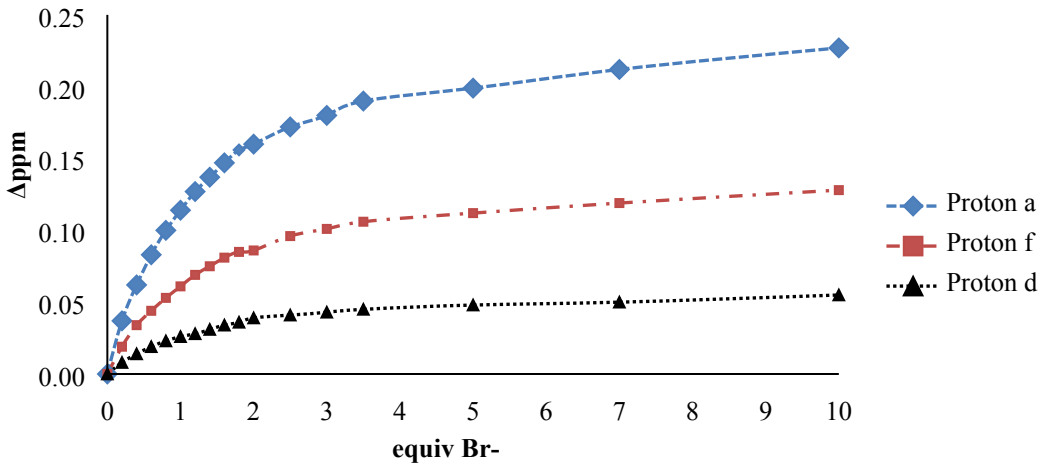

Figure S38. Plot of the data values from the titration study of [**1-H**](PF$_6$)with Br$^-$

c) Iodide titration

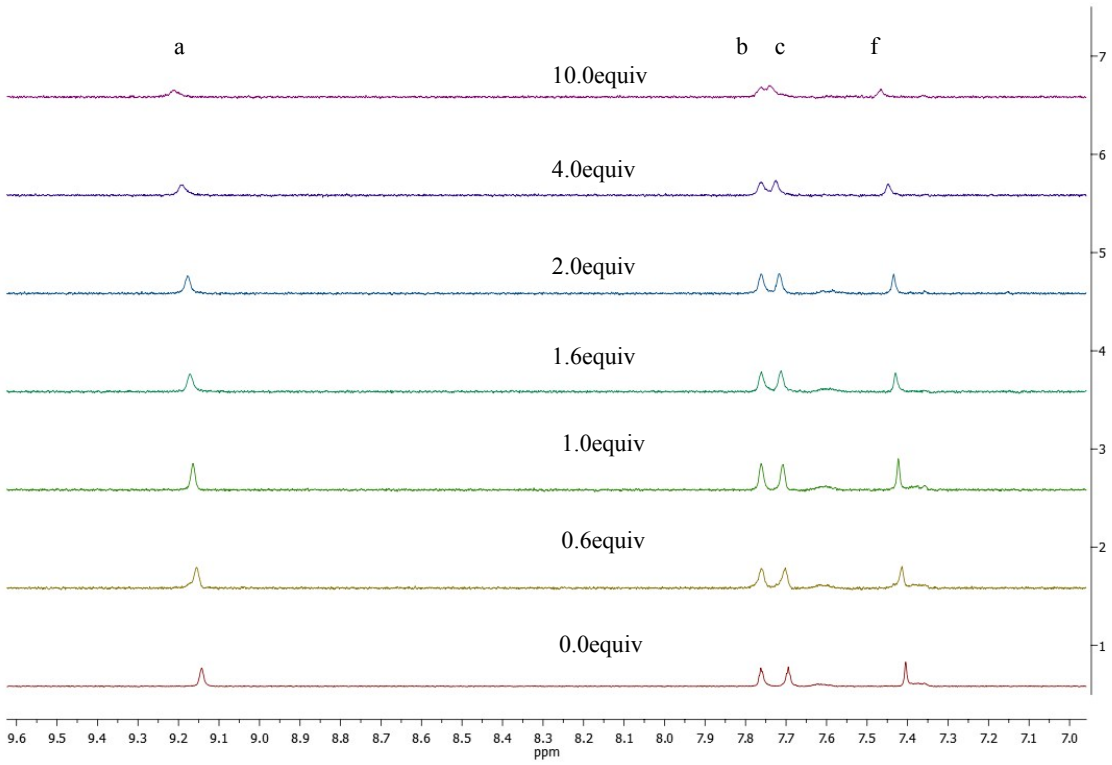

Figure S39. Partial ^{1}H NMR (400Hz) changes observed for the host [**1-H**](PF_6) in DMSO-d^6 during the addition of I^-.

Table S12: Data values from the titration study of **21(PF$_6$)$_3$** with I$^-$

[1-H](PF$_6$) (M)	equiv NBu4I	δa (ppm)	Δδa (ppm)	[NBu$_4$I] (M)
0,002	0,0	9,1308	0,0000	0
0,001992	0,2	9,1385	0,0077	0,000398
0,001984	0,4	9,1457	0,0149	0,000794
0,001976	0,6	9,1495	0,0187	0,001186
0,001969	0,8	9,1531	0,0223	0,001575
0,001961	1,0	9,1573	0,0265	0,001961
0,001953	1,2	9,1585	0,0277	0,002344
0,001946	1,4	9,1605	0,0297	0,002724
0,001938	1,6	9,1617	0,0309	0,003101
0,001931	1,8	9,1650	0,0342	0,003475
0,001923	2,0	9,1680	0,0372	0,003846
0,001905	2,5	9,1719	0,0411	0,004762
0,001887	3,0	9,1770	0,0462	0,00566
0,001869	3,5	9,1800	0,0492	0,006542
0,001818	5,0	9,1872	0,0564	0,009091
0,001754	7,0	9,1932	0,0624	0,012281
0,001667	10,0	9,2000	0,0703	0,016667

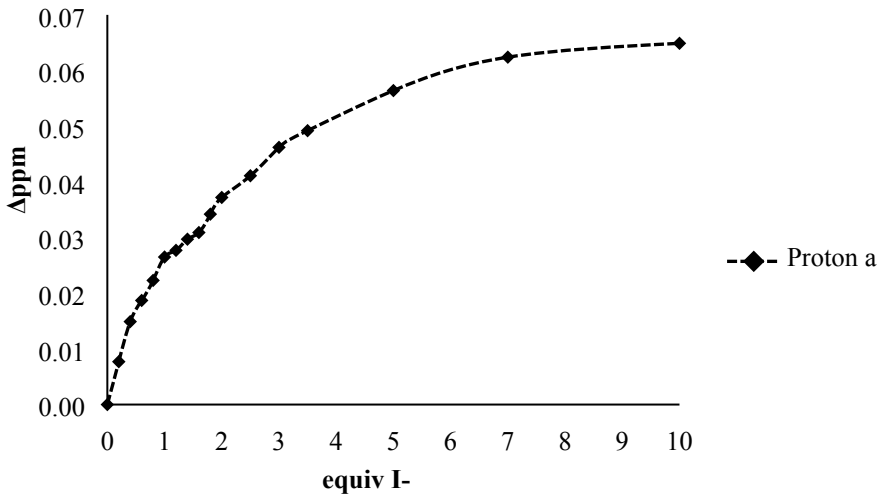

Figure S40. Plot of the data values from the titration study of [**1-H**](PF$_6$)with I$^-$

Titrations compound [**1-I**](PF_6)

a) Chloride titration

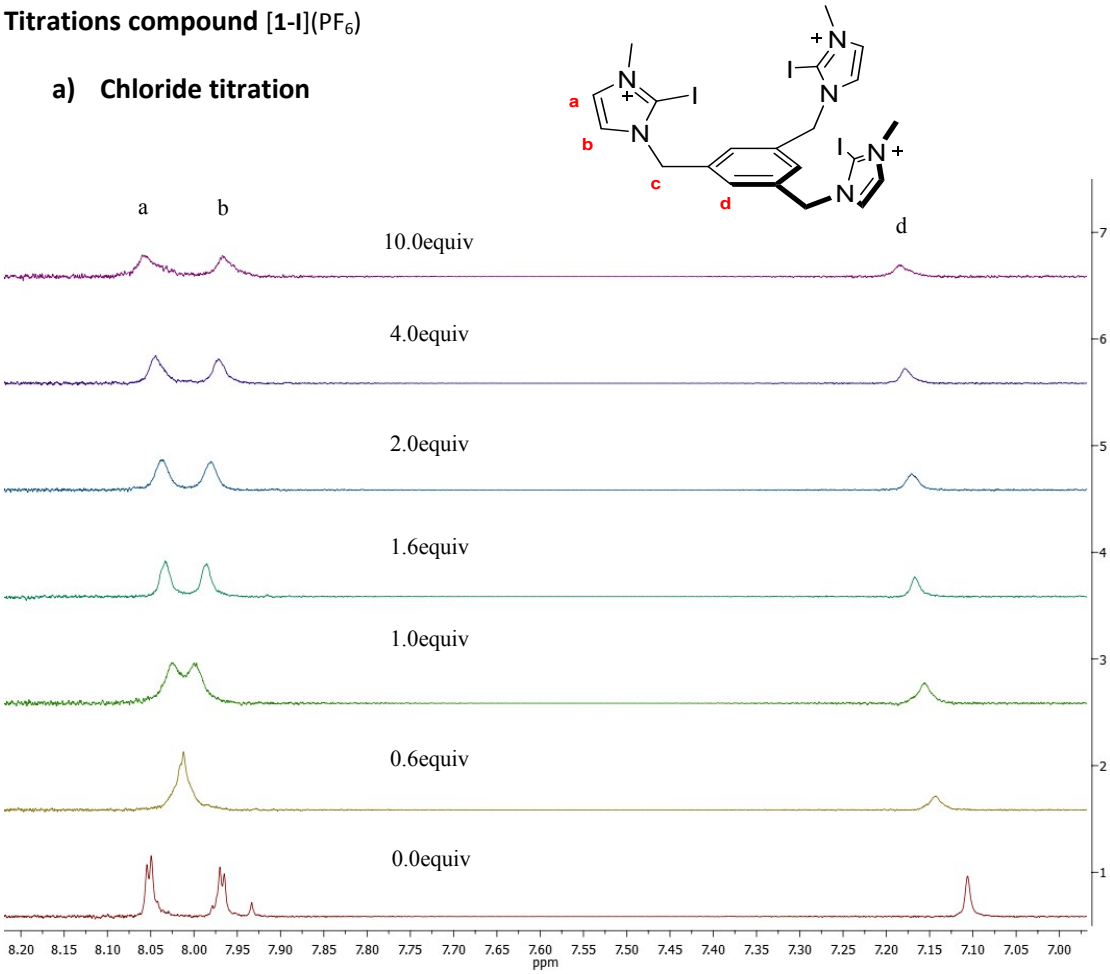

Figure S41. Partial ^{1}H NMR (400Hz) changes observed for the host [**1-I**](PF_6)in DMSO-d^6 during the addition of Cl^-.

Table S13. Data values from the titration study of **[1-I](PF$_6$)** with Cl$^-$

[1-I](PF$_6$) (M)	equiv NBu$_4$Cl	δa (ppm)	δf (ppm)	δd (ppm)	Δδa (ppm)	Δδf (ppm)	Δδd (ppm)	[NBu$_4$Cl] (M)
0,002	0,0	8,0437	7,9593	7,0986	0	0	0	0
0,001992	0,2	8,0320	7,9827	7,1084	-0,0113	0,0234	0,0098	0,000398
0,001984	0,4	8,0153	7,9964	7,1287	-0,0284	0,0371	0,0301	0,000794
0,001976	0,6	8,0030	8,0030	7,1343	-0,0407	0,0437	0,0357	0,001186
0,001969	0,8	8,0007	8,0141	7,1452	-0,043	0,0548	0,0466	0,001575
0,001961	1,0	7,9919	8,0183	7,1500	-0,0518	0,059	0,0514	0,001961
0,001953	1,2	7,9863	8,0217	7,1538	-0,0574	0,0624	0,0552	0,002344
0,001946	1,4	7,9829	8,0249	7,1577	-0,0608	0,0656	0,0591	0,002724
0,001938	1,6	7,9788	8,0259	7,1598	-0,0649	0,0666	0,0612	0,003101
0,001931	1,8	7,9768	8,0290	7,1623	-0,0669	0,0698	0,0637	0,003475
0,001923	2,0	7,9750	8,0311	7,1648	-0,0687	0,0718	0,0662	0,003846
0,001905	2,5	7,9702	8,0310	7,1661	-0,0735	0,0726	0,0675	0,004762
0,001887	3,0	7,9671	8,0330	7,1683	-0,0766	0,0744	0,0697	0,00566
0,001869	3,5	7,9638	8,0366	7,1704	-0,0799	0,0773	0,0718	0,006542
0,001818	5,0	7,9611	8,0414	7,1726	-0,0826	0,0821	0,074	0,009091
0,001754	7,0	7,9584	8,0430	7,1745	-0,0853	0,0837	0,0759	0,012281
0,001667	10,0	7,9559	8,0462	7,1750	-0,0878	0,0869	0,0764	0,016667

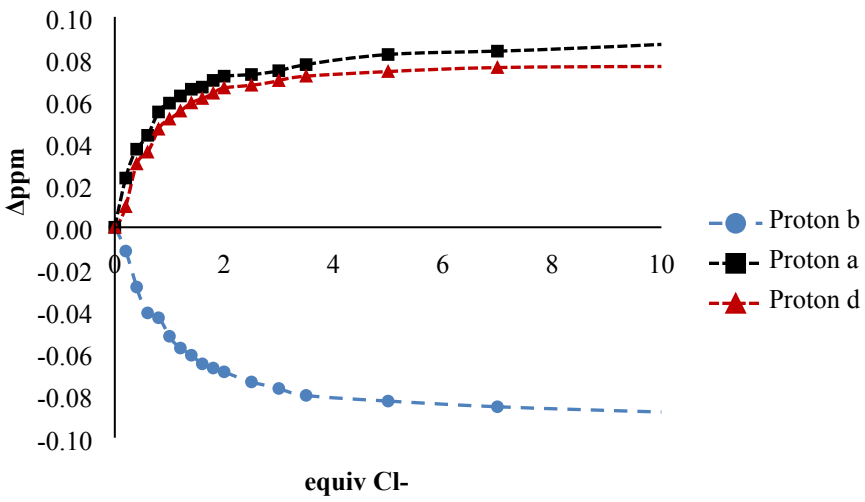

Figure S42. Plot of the data values from the titration study of [**1-I**](PF$_6$) with Cl$^-$

b) Bromide titration

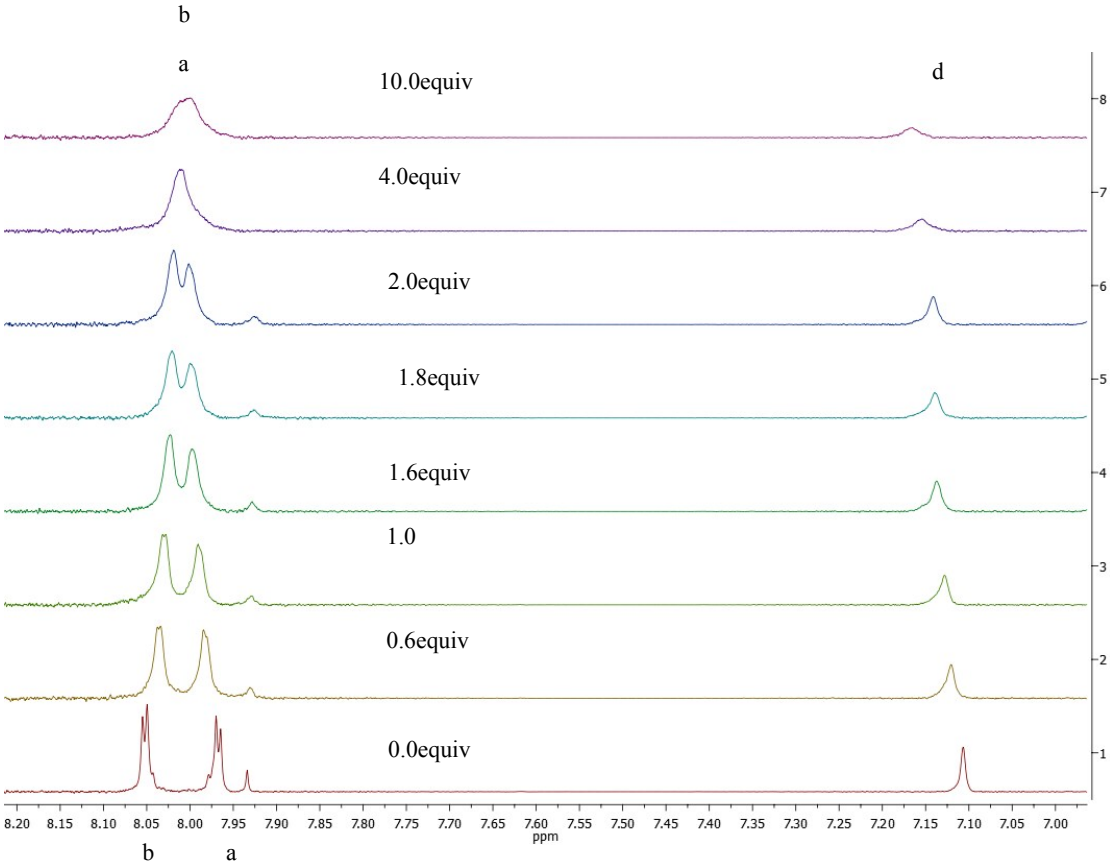

Figure S43. Partial ^{1}H NMR (400Hz) changes observed for the host [**1-I**](PF_6) in DMSO-d^6 during the addition of Br^-.

Table S14: Data values from the titration study of **[1-I](PF$_6$)** with Br$^-$

[1-I](PF$_6$) (M)	equiv NBu4Br	δa (ppm)	δb (ppm)	δd (ppm)	Δδa (ppm)	Δδb (ppm)	Δδd (ppm)	[NBu$_4$Br] (M)
0,002	0,0	8,0403	7,9553	7,0949	0	0	0	0
0,001992	0,2	8,0369	7,9673	7,1045	-0,0034	0,012	0,0096	0,000398
0,001984	0,4	8,0339	7,9721	7,1110	-0,0064	0,0168	0,0161	0,000794
0,001976	0,6	8,0299	7,9776	7,1145	-0,0104	0,0223	0,0196	0,001186
0,001969	0,8	8,0253	7,9790	7,1174	-0,015	0,0237	0,0225	0,001575
0,001961	1,0	8,0240	7,9834	7,1216	-0,0163	0,0281	0,0267	0,001961
0,001953	1,2	8,0205	7,9858	7,1248	-0,0198	0,0305	0,0299	0,002344
0,001946	1,4	8,0181	7,9879	7,1273	-0,0222	0,0326	0,0324	0,002724
0,001938	1,6	8,0162	7,9890	7,1297	-0,0241	0,0337	0,0348	0,003101
0,001931	1,8	8,0137	7,9903	7,1317	-0,0266	0,035	0,0368	0,003475
0,001923	2,0	8,0119	7,9920	7,1338	-0,0284	0,0371	0,0389	0,003846
0,001905	2,5	8,0086	7,9947	7,1374	-0,0317	0,0394	0,0425	0,004762
0,001887	3,0	8,0020	8,0020	7,1408	-0,0383	0,0467	0,0459	0,00566
0,001869	3,5	8,0020	8,0020	7,1450	-0,0383	0,0467	0,0501	0,006542
0,001818	5,0	8,0020	8,0020	7,1485	-0,0383	0,0467	0,0536	0,009091
0,001754	7,0	8,0020	8,0020	7,1537	-0,0383	0,0467	0,0588	0,012281
0,001667	10,0	8,0020	8,0020	7,1591	-0,0383	0,0467	0,0642	0,016667

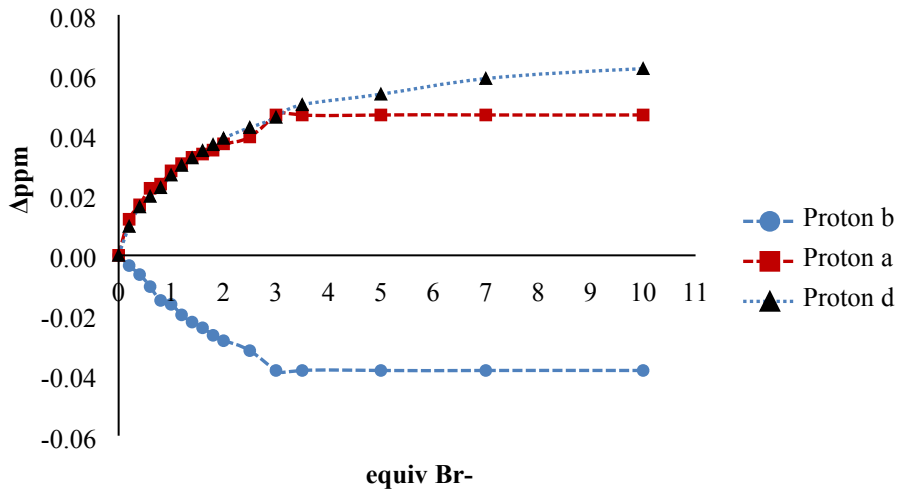

Figure S44. Plot of the data values from the titration study of [**1-I**](PF$_6$)with Br$^-$

c) Iodide titration

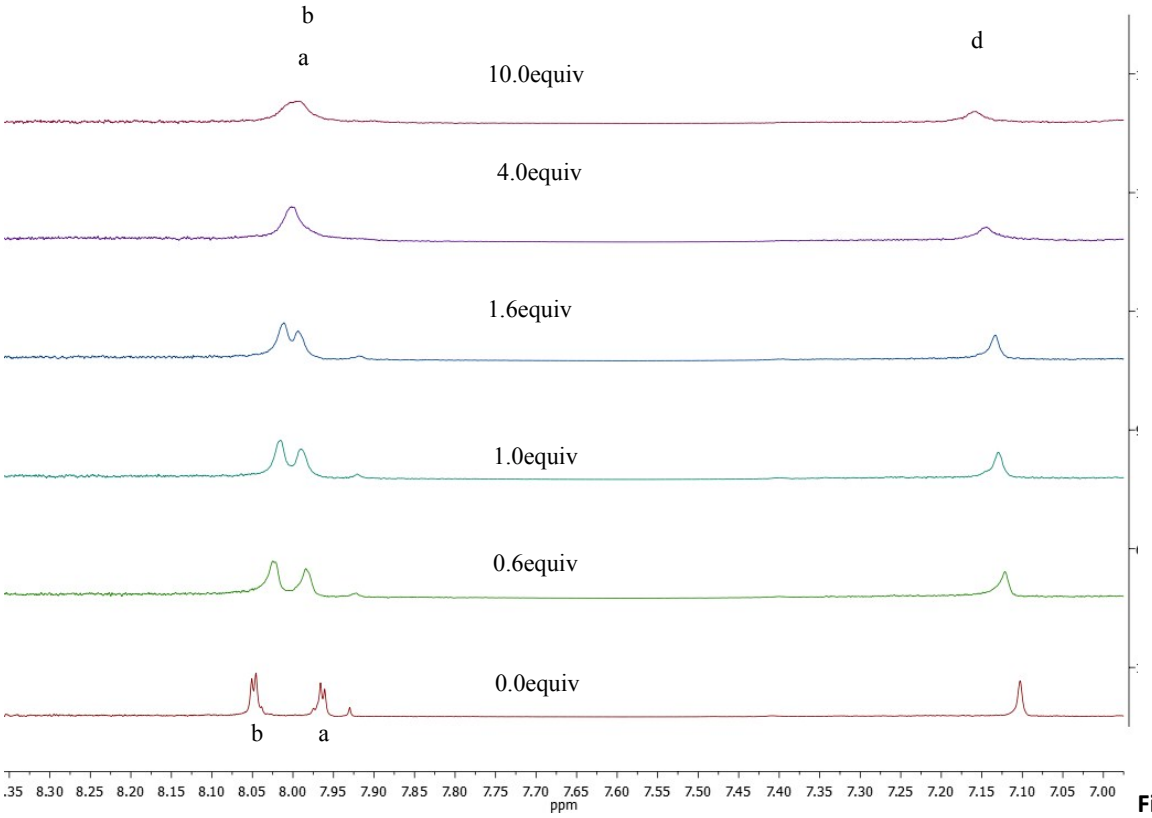

Figure S45. Partial ^{1}H NMR (400Hz) changes observed for the host [**1-I**](PF_6)in DMSO-d^6 during the addition of I^-

Table S15: Data values from the titration study of **[1-I](PF$_6$)**with I$^-$

[1-I](PF$_6$) (M)	equiv NBu4I	δa (ppm)	Δδa (ppm)	[NBu$_4$I] (M)
0,002	0,0	7,1029	0,0000	0
0,001992	0,2	7,1040	0,0016	0,000398
0,001984	0,4	7,1110	0,0081	0,000794
0,001976	0,6	7,1145	0,0116	0,001186
0,001969	0,8	7,1174	0,0145	0,001575
0,001961	1,0	7,1216	0,0187	0,001961
0,001953	1,2	7,1248	0,0219	0,002344
0,001946	1,4	7,1273	0,0244	0,002724
0,001938	1,6	7,1297	0,0268	0,003101
0,001931	1,8	7,1317	0,0288	0,003475
0,001923	2,0	7,1338	0,0309	0,003846
0,001905	2,5	7,1374	0,0345	0,004762
0,001887	3,0	7,1408	0,0379	0,00566
0,001869	3,5	7,1460	0,0431	0,006542
0,001818	5,0	7,1485	0,0456	0,009091
0,001754	7,0	7,1530	0,0501	0,012281
0,001667	10,0	7,1545	0,0516	0,016667

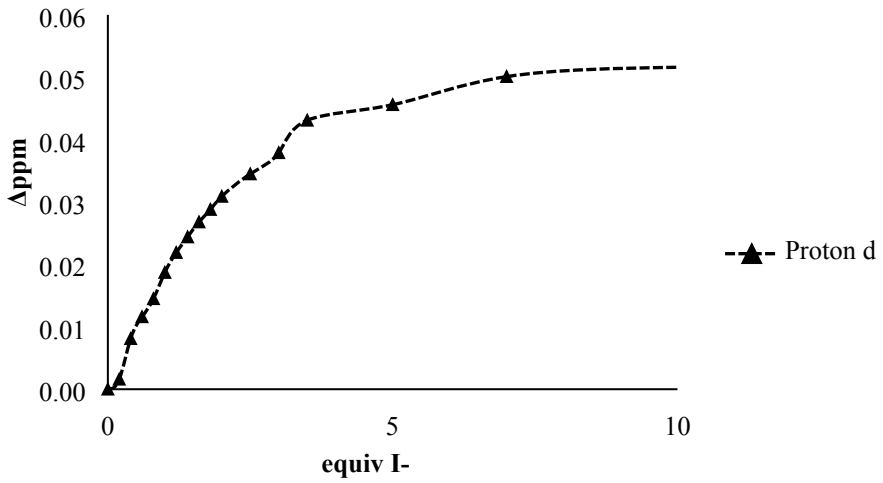

Figure S46. Plot of the data values from the titration study of [**1-I**](PF$_6$)with I$^-$

d) Dihydrogen phophate titration

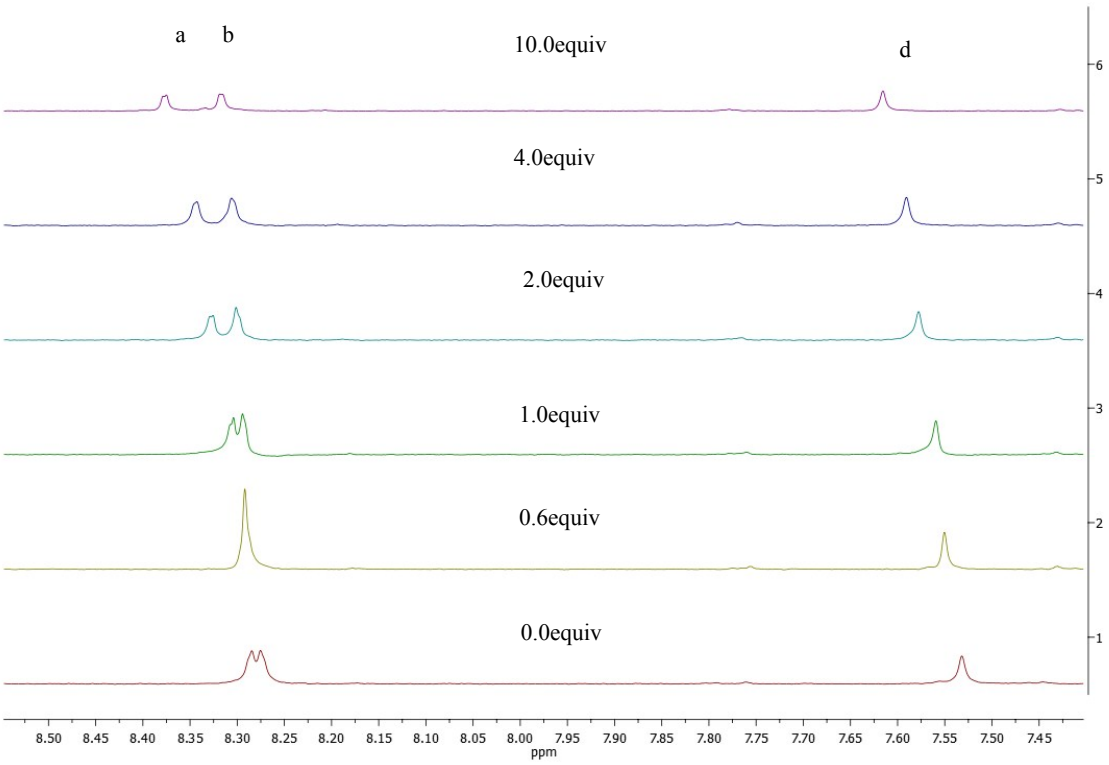

Figure S47. Partial ^{1}H NMR (400Hz) changes observed for the host [**1-I**](PF_6) in DMSO-d^6:D_2O during the addition of $H_2PO_4^-$

Table S16: Data values from the titration study of **[1-I](PF$_6$)**with $H_2PO_4^-$

[1-I](PF$_6$) (M)	equiv $NBu_4H_2PO_4$	δb (ppm)	δd (ppm)	Δδb (ppm)	Δδd (ppm)	[$NBu_4H_2PO_4$] (M)
0,002	0,0	8,2759	7,5323	0	0	0
0,001992	0,2	8,2855	7,5386	0,0096	0,0063	0,000398
0,001984	0,4	8,2890	7,5447	0,0131	0,0124	0,000794
0,001976	0,6	8,2919	7,5504	0,016	0,0181	0,001186
0,001969	0,8	8,2930	7,5549	0,0171	0,0226	0,001575
0,001961	1,0	8,3039	7,5594	0,028	0,0271	0,001961
0,001953	1,2	8,3069	7,5635	0,031	0,0312	0,002344
0,001946	1,4	8,3132	7,5666	0,0373	0,0343	0,002724
0,001938	1,6	8,3167	7,5709	0,0408	0,0386	0,003101
0,001931	1,8	8,3222	7,5741	0,0463	0,0418	0,003475
0,001923	2,0	8,3257	7,5777	0,0498	0,0454	0,003846
0,001905	2,5	8,3291	7,5806	0,0532	0,0483	0,004762
0,001887	3,0	8,3354	7,5850	0,0595	0,0527	0,00566
0,001869	3,5	8,3380	7,5906	0,0621	0,0583	0,006542
0,001818	5,0	8,3449	7,5977	0,069	0,0654	0,009091
0,001754	7,0	8,3540	7,6042	0,0781	0,0719	0,012281
0,001667	10,0	8,3550	7,6042	0,0791	0,07192	0,016667

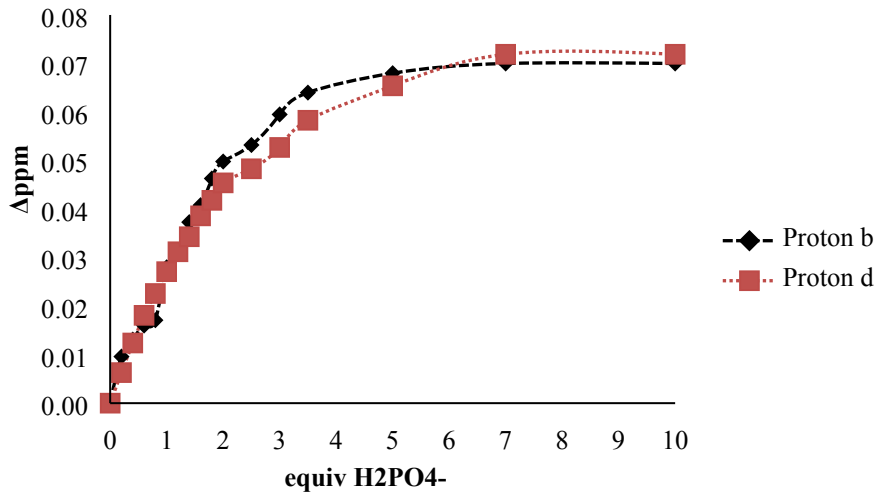

Figure S48. Plot of the data values from the titration study of [**1-I**](PF$_6$)with $H_2PO_4^-$

S8. COMPUTATIONAL STUDIES

Classical molecular dynamics (MD) simulations.

Explicit solvent classical molecular dynamics (MD) simulations were performed at constant temperature (300 K) and pressure (1 atm) using the NAMD code. Electroneutral models were build including the receptor and three counterions (either Cl^- or PF_6^-). Cubic simulation cells of 47 – 49 Å side including about 900 DMSO molecules were used. A cutoff of 12 Å was used for Van der Waals interactions and the real part of electrostatic interactions. The particle mesh Ewald method was used to treat long range electrostatics on a cubic grid of 64^3 points.[1] All bonds involving H were constraint.[2]

Force field parameters for the DMSO solvent and chloride anions were available from the AMBER distribution[3] Atomic charges for PF_6^- and the receptors were determined according the RESP procedure.[4] For the receptors, an open conformation was used for charge fitting and equivalence of the receptor's arms was imposed. Bonding parameters were available through the GAFF force field.[5] In the case of the iodoimidazolium based receptor, a parametrization to reproduce halogen bonding at iodine was adapted from Jorgensen and Schyman article.[6] Accordingly, a psuedo-atom (X) of +0.2e charge was placed along the C – I axis at a distance of 1.8 Å from I and harmonic potentials were used to restraint the I – X distance (1.8 Å, force constant 600 kcal mol^{-1} $Å^{-2}$) and C – I – X angle (linear, force constant 200 kcal $mol^{-1}deg^{-2}$). This set of parameters reproduce structural features of a reduced model system (Figure S49), slightly overestimating the I – Cl distance.

Quantum chemical calculations.

Quantum chemical calculations were performed using the ORCA software and based on Density Functional Theory (DFT). The B3LYP functional was used to describe electron exchange and correlation.[7] A SVP basis set was used for geometry optimization and TZVP for single point energy evaluation.[8] Relativistic effects were accounted for using the ZORA approximation. Solvent effects were accounted using the COSMO implicit solvent model.[9] The counterpoise correction was used to correct binding energies for the basis set superposition error.[10]

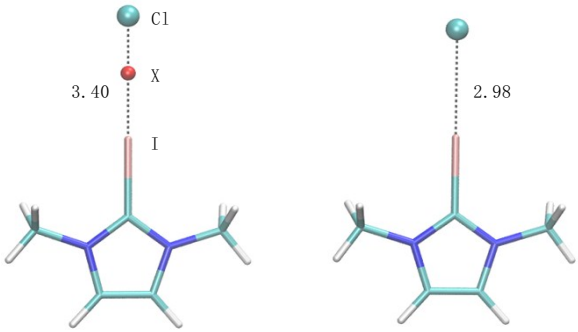

Figure S49. Molecular mechanics (left panel) and DFT (right panel) optimized structures of model iodoimidazolium / chloride complex. The I – Cl distance is shown in Å

Molecular modeling of the* [1-H]$^{3+}$ */ anion system

Molecular dynamics simulations of the **[1-H]$^{3+}$** receptor were performed in explicit DMSO solvent to characterize the conformational dynamics of the receptor and its interactions with counterions. Independent simulations for PF_6^- and Cl^- counterions were performed. About 100 ns simulations were collected for each system.

a) Conformational analysis.

Each arm of the imidazolium receptor has two rotable bonds, potentially giving rise to a high number of conformers. In the present context, the relative distance and orientation of the arms may be used to characterize the receptor conformation. It may be appreciated from Figure S50 that the distribution of distances between the arms of the receptor is markedly dependent on the nature of the counterion (X). For both anions, inter-arm distances display similar distributions, supporting convergence of the simulations and showing that the length of the simulation is appropriate for the present purposes. For X=PF_6^-, broad distributions are observed, whereas for X=Cl^- sharper peaks are displayed at shorter distance (about 7 Å). Furthermore, variation of the inter-arm distances appear correlated for X=Cl^-. These data are suggestive of a structuring of the receptor induced by Cl^-, but not by PF_6^-.

b) Binding analysis

The interactions of $Cl^-$and PF_6^- anions with the receptor are markedly different. In the case of Cl^-, interactions with the N*C*N carbon and the methyl carbon are favored compared to other carbon atoms of the imidazolium rings or of the benzene scaffold. On the contrary, PF_6^- does not display to favor specific interactions with any of the carbon atoms of the receptor. Figure S52 shows the distances between the chloride anions and the N*C*N carbon atoms of the imidazolium rings. It may be appreciated that one of the chloride anions (Cl_2) interacts simultaneously with the three arms of the receptor for about 50 ns in the central part of the simulation. Only occasionally one of the

interactions is broken. Similarly, Cl_3 interacts with two or three receptor's arms in the initial 30 ns of the simulation. Worth noting that along the simulation two chloride anions may be found close to the receptor at the same time. However, it appears that one is bound more strongly than the other, which displays short lived interactions. Figure S54 shows a representative snapshot from the simulation of a tri-coordinated chloride anion, which interacts with the N*C*N carbon and the methly groups of the three receptor's arms simultaneously. In the case of PF_6^- no such long lasting interactions were observed (Figure S53).

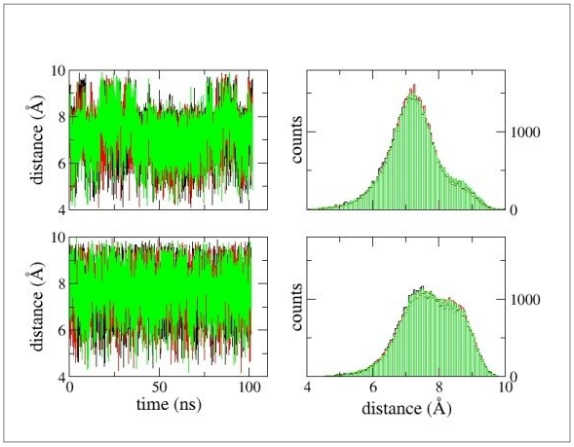

Figure S50. MD simulation of **[1-H]**$(X)_3$. Distances between the centers of the imidazolium rings of the receptor's arms. Top graphs for **[1-H]**$(Cl)_3$, bottom ones for **[1-H]**$(PF_6)_3$. Left graphs are the time, right ones the corresponding histograms

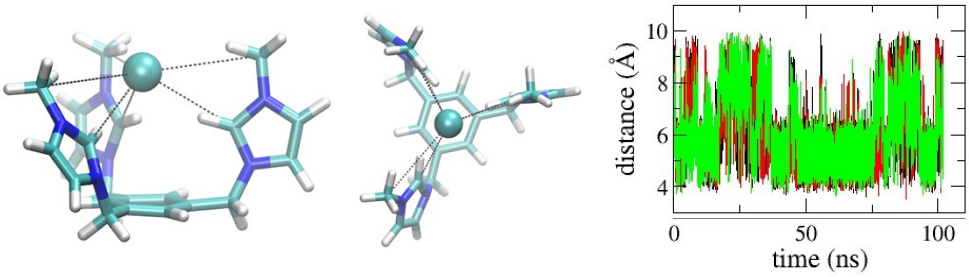

Figure S51. Side and top views of the receptor – chloride complex at about 50 ns MD simulation of **[1-H]**$(Cl)_3$. On the right, the time series of the distances between the N*C*N carbons of the imidazolium rings of the receptor's arms are shown.

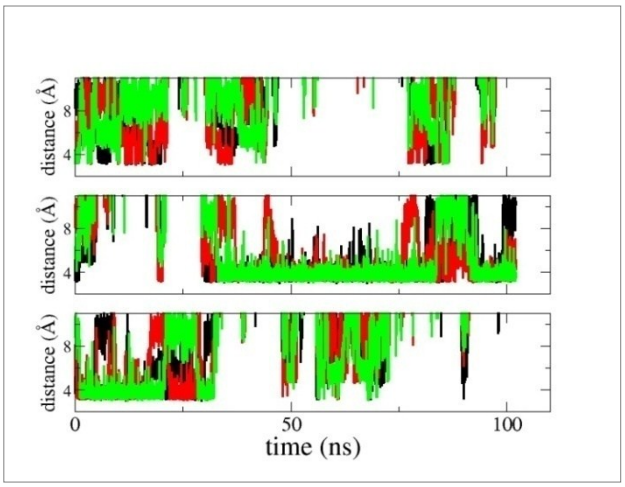

Figure S52. MD simulation of **[1-H]**$(Cl)_3$. Distances between the chloride anions (one graph per anion) and the N*C*N carbon of the imidazolium rings of the receptor's arms (one curve per arm in each graph)

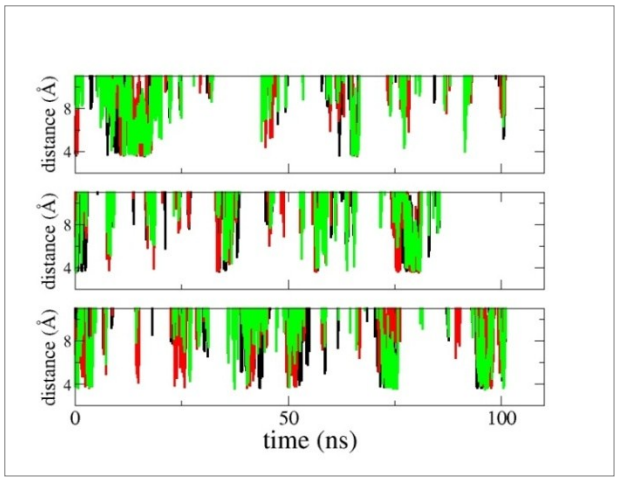

Figure S53. MD simulation of **[1-H]$(PF_6)_3$**. Distances between the phosphorous atom of the hexafluorophosphate anions (one graph per anion) and the N*C*N carbon of the imidazolium rings of the receptor's arms (one curve per arm in each graph)

Molecular modeling of the* [1-I]$^{3+}$ */ anion system

Molecular dynamics simulations were performed to for receptor **[1-I]$^{3+}$** $^{+}$ in explicit DMSO solvent to characterize the conformational dynamics of the receptor and its interactions with counterions. Simulations were performed starting from different conformations of the receptor and combinations of counterions. About 100 ns simulations were collected for each system.

a) Conformational analysis.

As for the **[1-H]$^{3+}$** receptor, the nature of the counterion has a considerable impact on the conformational properties of the **[1-I]$^{3+}$** $^{+}$ receptor. When PF_6^- is the counterion, similar distributions are observed for the inter-arm distances (Figure S54). On the contrary, when (at least one) Cl^- is present a marked correlation is observed for the motion of two receptor's arms due to the stable interactions formed between chloride and two C – I moieties. A cluster analysis revealed three populated conformational states (Figure S55). The conformation labeled as **c** in Figure S55 is responsible for the shoulders in the distributions of inter-arm distances reported in Figure S54.

b) Binding analysis.

In the simulation of **[1-I](PF_6)$_3$**, PF_6^- displayed unspecific and short lived interactions with the receptor (Figure S60), as observed for the **[1-H]$^{3+}$** receptor. On the contrary, highly stable interactions formed between the receptor's arms and Cl anions. Simulations **[1-I](Cl)$_3$_i** (Figure S56) and**[1-I]**(Cl)$_3$_ii (Figure S58) showed two preferred binding modes of Cl anions, one involving two receptor's arms and another in which only one receptor arm binds Cl. These interactions are maintained throughout the simulations. Simulation **[1-I](Cl)$_3$_ii** was started from a tri-coordinated Cl, but this interaction mode was maintained only for the first 7 ns (Figure S58), then one of the arms detached from Cl and bound a second Cl anion (this result is in line with the outcome of quantum chemical calculations, see below). Model **[1-I](Cl)(PF_6)$_2$**, was used to investigate the effect of anion composition on the receptor's properties. The simulation was started from a tri-coordinated Cl binding, which however was maintained only during the first few ns, then reverting to a two-coordinated conformation (Figure S59). Worth noting in Figures S56, S58 and S59 is the occurrence of short lived interactions with a third receptor's arm. However, these do not involve the C – I unit (see Figure S57).

Quantum chemical calculations were performed to compare the energetics of the different binding modes of chloride anions to the **[1-I]$^{3+}$** receptor. Representative structures from the MD simulations were optimized and used to compare the energetics of Cl binding to one, two and three arms of the receptor. Successive binding of the arm's receptor is favorable (Table S17). However, passing from two to three arm's coordination the gain in stability is small, due to the cost of bringing together the positively charged arms. Indeed, the energy difference between the open and closed conformations

is 9.9 kcal mol^{-1} in favor of the open structure (Figure S62, which is about the binding energy of Cl^- to iodoimidazolium (-10.6 kcal mol^{-1}, Figure S63).

We have further compared the energies of the receptor interacting with two Cl^- in different conformations (Figure S61). In line with the above results and those from the MD study, binding of one Cl to two arms and one to one arm (Figure S61.b,c) is favored compared to binding of one Cl to three arms and one Cl interacting unspecifically with the receptor (Figure S63.a). Quantum chemical calculations were used to compare the strength of anion···HC and anion···IC interactions. The optimized geometries of the model compounds are shown in Figure S63 together with the estimated binding energy. Binding based on halogen bonding is favored by 3.2 kcal mol^{-1}.

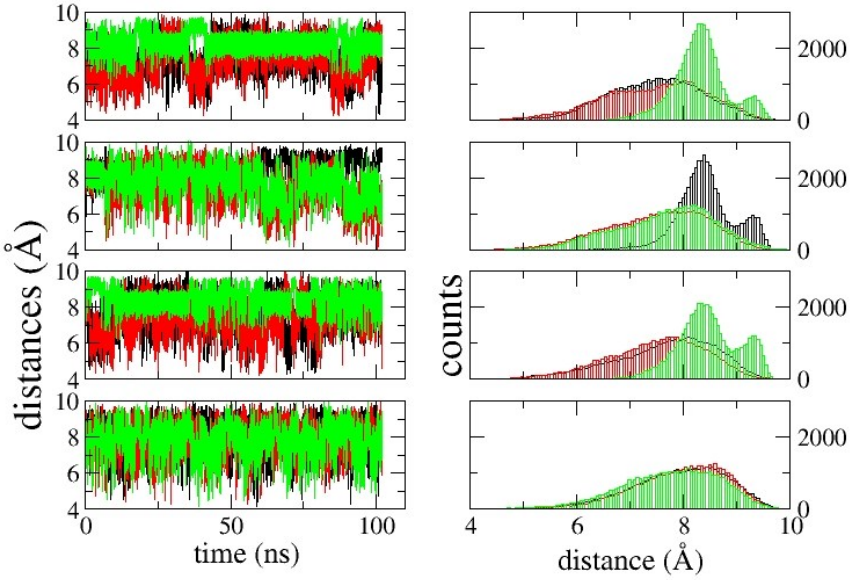

Figure S54. MD simulation of **[1-I]**$(X)_3$. Distances between the centers of the iodoimidazolium rings of the receptor's arms. From top to bottom: **[1-I]$(Cl)_3$_i**, **[1-I]$(Cl)_3$_ii**, **[1-I]$(Cl)(PF_6)_3$**, **[1-I]$(PF_6)_3$**. Left graphs are the time series, right ones the corresponding histograms

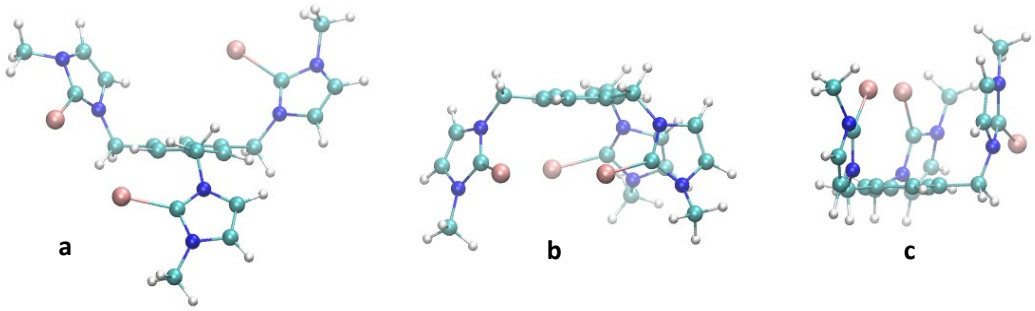

Figure S55. Representative snapshots of **[1-I]$^{3+}$** from the MD simulation of model **[1-I]$(Cl)_3$**

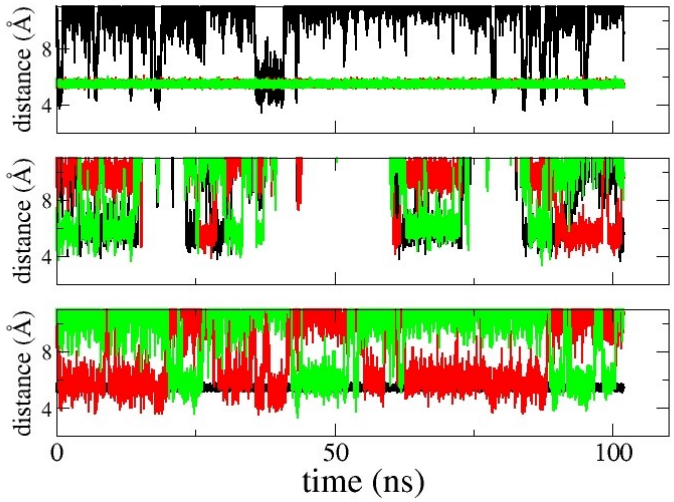

Figure S56. MD simulation of **[1-I](Cl)$_3$_i**. Distances between the chloride anions (one graph per anion) and the N*C*N carbon of the iodoimidazolium rings of the receptor's arms (one curve per arm in each graph)

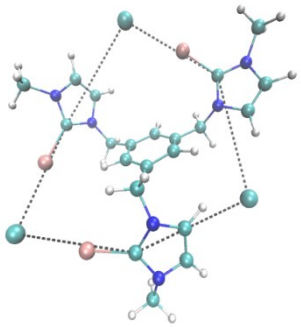

Figure S57. Snapshot at 66 ns simulation of the **[1-I](Cl)$_3$** model. Dotted lines highlight selected distance, all of them of similar length (about 5.5 Å)

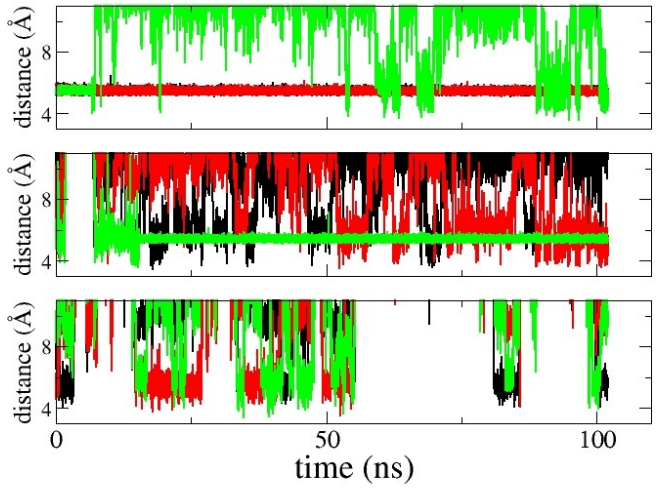

Figure S58. MD simulation of **[1-I](Cl)$_3$_ii.** Distances between the chloride anions (one graph per anion) and the N*C*N carbon of the iodoimidazolium rings of the receptor's arms (one curve per arm in each graph)

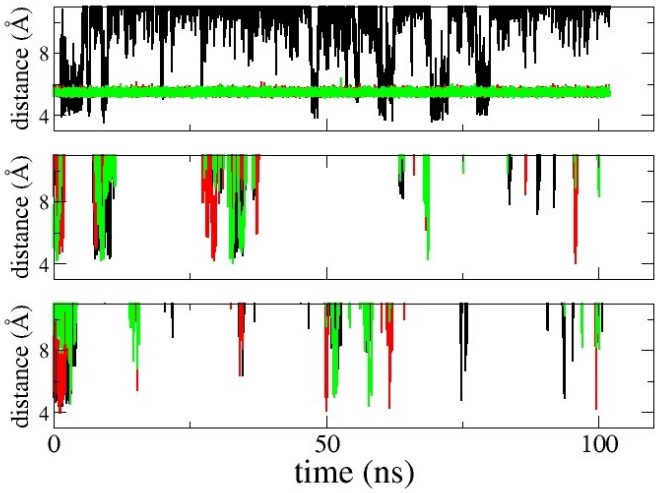

Figure S59. MD simulation of **[1-I](Cl)(PF$_6$)$_2$.** Distances between the anions (one graph per anion; top: Cl^-, middle and bottom: PF_6^-) and the N*C*N carbon of the iodoimidazolium rings of the receptor's arms (one curve per arm in each graph)

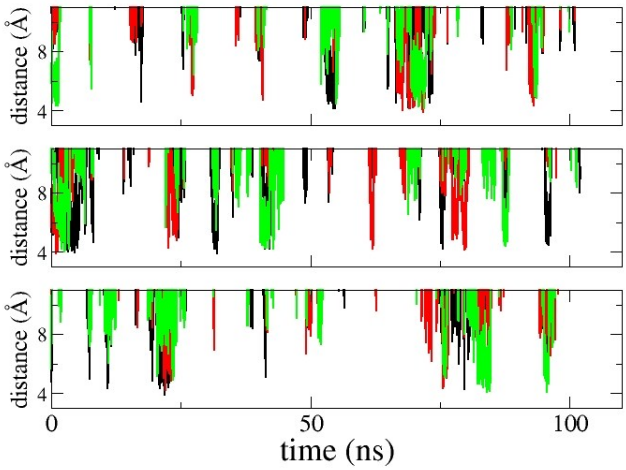

Figure S60. MD simulation of **[1-I](PF_6)$_3$**. Distances between the phosphorous atom of the hexafluorophosphate anions (one graph per anion) and the NCN carbon of the iodoimidazolium rings of the receptor's arms (one curve per arm in each graph)

Table S17. Conformational energies of the **[1-I]$^{3+}$** receptor interacting with one chloride anion. Energies were estimating based on the conformations shown in Figure S61 removing one of the Cl anions

number of arms interacting with Cl^-	Energy (kcal mol^{-1})
1	6.4
2	1.7
3	0.0

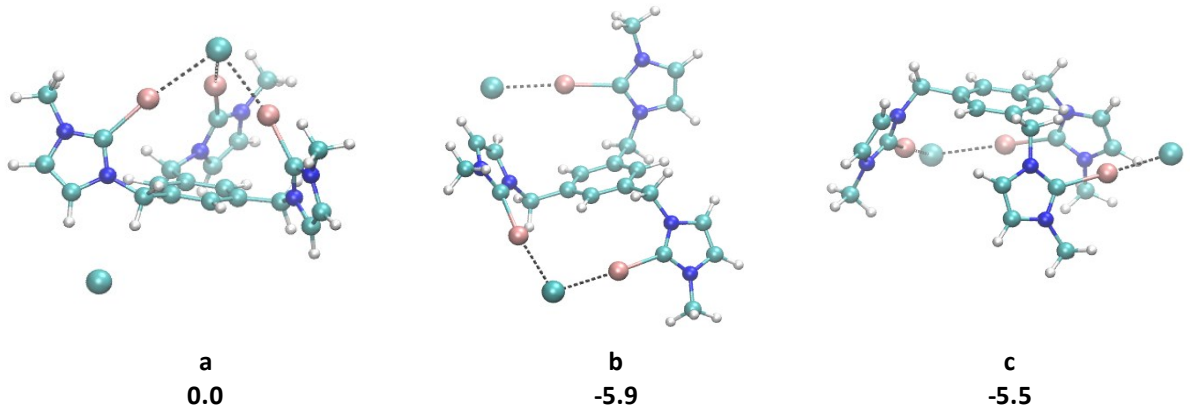

Figure S61. Different binding modes of two Cl anions to the **[1-I]$^{3+}$** receptor. The binding shown in **b** and **c** differ for the orientation of the arms, in **c** being all three on the same side of the benzene plane. Energies are reported in kcal mol^{-1}

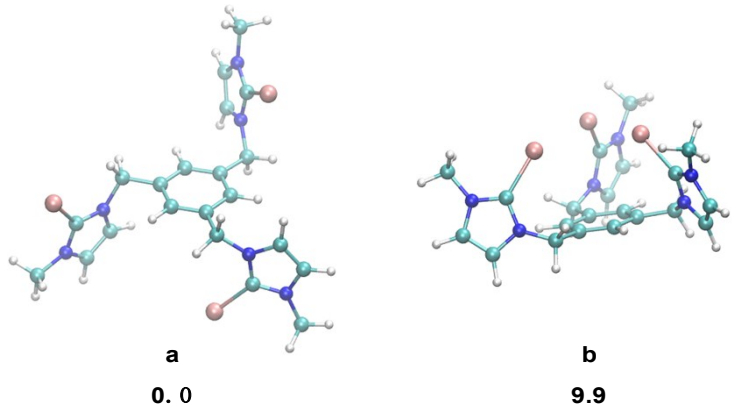

Figure S62. Different conformations of receptor **[1-I]$^{3+}$.** The conformation in **a** is fully optimized without the presence of any counterions. The conformation shown in **b** does not correspond to a stable minimum. Energies are reported in kcal mol^{-1}

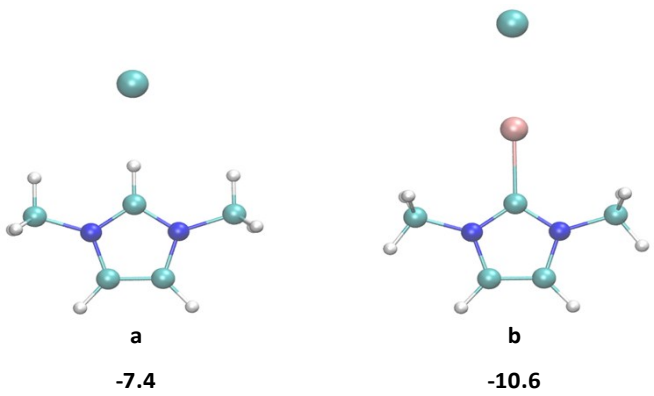

Figure S63. Model compounds used to estimate the binding energy of Cl^- to imidazolium (a) and iodoimidazolium (b). Energies (corrected for the basis set superpositon error) are reported in kcal mol^{-1}

S.9. Crystal Structure of compound [1-I]$^{3+}$

Crystals suitable for X-ray study of compound **[1-I]$^{3+}$**, were obtained by slow diffusion of methanol into a concentrated solution of **[1-I](BF$_4$)** (with one equivalent of TBACl) in chloroform. Diffraction data was collected on an Agilent SuperNova diffractometer equipped with an Atlas CCD detector using Mo-Kα radiation (λ= 0.71073 Å). Single crystals were mounted on a MicroMount® polymer tip (MiteGen) in a random orientation. Absorption corrections based on the gaussian method were applied. Using Olex2[11] the structures of all the complexes were solved using Charge Flipping[12] in Superflip and refined with ShelXL[13] refinement package using Least Squares minimisation. Key details of the crystals and structure refinement data are summarized in Supplementary Table S18. Further crystallographic details may be found in the CIF files, which were deposited at the Cambridge Crystallographic Data Centre, Cambridge, UK. The reference number for compound **[1-I](BF$_4$)** was assigned as 1521906.

Table S18: Crystallographic data and structure refinement for compound **[1-I](BF$_4$)**

	[1-I]BF$_4$
Empirical formula	$C_{22}H_{23}B_2Cl_4F_8I_3N_6$
Formula weight	1067.58
Temperature/K	200.00(14)
Crystal system	orthorhombic
Space group	Pbca
a/Å	13.6312(2)
b/Å	23.5061(4)
c/Å	24.2909(4)
α/°	90
β/°	90
γ/°	90
Volume/Å^3	7783.2(2)
Z	4
ρ_{calc}g/cm^3	1.822
μ/mm^{-1}	2.746
F(000)	4048.0
Crystal size/mm	24.2909 × 23.5061 × 13.6312
Radiation	MoKα (λ = 0.71073)
2Θ range for data collection/°	5.674 to 57.832
Index ranges	$-17 \leq h \leq 18$, $-28 \leq k \leq 31$, $-32 \leq l \leq 33$
Reflections collected	77836
Independent reflections	9735 [R_{int} = 0.0357, R_{sigma} = 0.0236]
Data/restraints/parameters	9735/0/431
Goodness-of-fit on F^2	1.053
Final R indexes [I>=2σ (I)]	R_1 = 0.0359, wR_2 = 0.0856
Final R indexes [all data]	R_1 = 0.0537, wR_2 = 0.0978
Largest diff. peak/hole / e Å^{-3}	1.05/-1.01

S10. References

(1) Darden, T., York, D., Pedersen, L. *J. Chem. Phys.* **1993**, *98*, 10089-10092.
(2) Ryckaert, J. P., Ciccotti, G., Berendsen, H. J. C. *J. Comput. Phys.* **1977**, *23*, 327-341.

(3) Fox, T., Kollman, P. A. *J. Phys. Chem. B* **1998**, *102*, 8070-8079.
(4) Bayly, C. I., Cieplak, P., Cornell, W. D., Kollman, P. A. *J. Phys. Chem.* **1993**, *97*, 10269-10280.
(5) Wiberg, K. B., Wang, Y. G. *J. Comput. Chem.* **2004**, *25*, 1127-1132.
(6) Jorgensen, W. L., Schyman, P. *J. Chem. Theory Comput.* **2012**, *8*, 3895-3901.
(7) Becke, A. D. *J. Chem. Phys.* **1993**, *98*, 5648-5652.
(8) Pantazis, D. A., Chen, X. Y., Landis, C. R., Neese, F. *J. Chem. Theory Comput.* **2008**, *4*, 908-919.
(9) Klamt, A., Schuurmann, G. *J. Chem. Soc., Perkin Trans. 2* **1993**, 799-805.
(10) Boys, S. F., Bernardi, F. *Mol. Phys.* **1970**, *19*, 553-556.
(11) Dolomanov, O. V., Bourhis, L. J., Gildea, R. J., Howard, J. A. K., Puschmann, H. *J. Appl. Crystallogr.* **2009**, *42*, 339-341.
(12) a) Palatinus, L., Chapuis, G. *J. Appl. Crystallogr.* **2007**, *40*, 786-790; b) Palatinus, L., Prathapa, S. J., van Smaalen, S. *J. Appl. Crystallogr.* **2012**, *45*, 575-580; c) Palatinus, L., van der Lee, A. *J. Appl. Crystallogr.* **2008**, *41*, 975-984.
(13) Sheldrick, G. M. *Acta Crystallographica a-Foundation and Advances* **2015**, *71*, 3-8.